LAWRENCE
LIVERMORE
NATIONAL
LABORATORY

LLNL-CONF-514891

Compression Molding of UF-TATB with Various Mold Releases

M. Gresshoff, D. M. Hoffman

November 18, 2011

Insensitive Munitions and Energetic Materials
Las Vegas, NV, United States
May 14, 2012 through May 17, 2012

Disclaimer

This document was prepared as an account of work sponsored by an agency of the United States government. Neither the United States government nor Lawrence Livermore National Security, LLC, nor any of their employees makes any warranty, expressed or implied, or assumes any legal liability or responsibility for the accuracy, completeness, or usefulness of any information, apparatus, product, or process disclosed, or represents that its use would not infringe privately owned rights. Reference herein to any specific commercial product, process, or service by trade name, trademark, manufacturer, or otherwise does not necessarily constitute or imply its endorsement, recommendation, or favoring by the United States government or Lawrence Livermore National Security, LLC. The views and opinions of authors expressed herein do not necessarily state or reflect those of the United States government or Lawrence Livermore National Security, LLC, and shall not be used for advertising or product endorsement purposes.

Compression Molding of UF-TATB with Various Mold Releases

M. Gresshoff[1] and D. M. Hoffman[2]*
Defense Technologies Engineering Department[1]
Energetic Materials Center High Explosives Application Facility[2]
Lawrence Livermore National Laboratory
Livermore, CA 94550

6/22/11

Abstract

The insensitive high explosive 1,3,5-triamino-2,4,6-trinitrobenzene, TATB, with an average particle size of about 6 μm, called ultra-fine, was compression molded into 1.27 dia. x 2.54 cm right circular cylinders at 200 MPa under load control at a rate of 2.7 kg/s with a series of 12 mold release agents. Cylinder density varied between 1.92-1.88 gm/cc in the press based on ram displacement with between 4.0-1.5% spring back as the pressure was released. For a single cycle with a 2-minute hold, the final part densities varied between 1.839-1.843 gm/cc. This density difference was not significant enough to differentiate release agents. After the cylinder had been molded, the force required to extract it from the mold varied depending on the release agent from almost 800 to 2200 N (180 to 500 lbf). This translates to extraction pressures between 6.5 to 10 MPa (950 to 1450 psi). About 1400 N (320 lbf) was required to extract TATB without mold release, so some release agents were worse than none and some significantly better. X-ray CT scans were run on86 of the parts to identify density distributions. These also showed that when powders, such as talc, are used, residue is incorporated in the sides of the cylinders.

Introduction

Compression molding is the most convenient method for processing explosives and other crystalline solids into simple shapes. Studies of powder compaction of ceramics [1, 2], metals [3, 4], pharmaceuticals [5-9], polymers[10-12], explosives[13-15] and other organic materials[16-18] have been described in the literature. Three main problems arise from compression molding organic materials: 1. Poor densification or density distribution, 2. Cracks and 3. Internal voids. Variation in density along the pressure direction is usually associated with inter-granular and wall friction, so density uniformity is expected to increase as wall friction is reduced [19]. Density variation in initiator or booster explosives is a problem because the detonation velocity is directly proportional to the density[20, 21]. This can alter the breakout timing and the lighting of the main charge. [22] Since lubrication is used extensively industrially, different commercial mold releases were evaluated to mitigate this problem. Cracks in single-cycle ultrafine TATB and other compression molded explosives have been observed either during extraction from the die or shortly after molding. Voids can result from poor packing or insufficient pressure to cause the material to yield and flow. Many characterization techniques have been used to probe the details of cracking, voids and density distribution. [6, 8, 23, 24] Radiography has been used extensively at LLNL for this purpose and several samples were investigated using x-ray computer tomography (X-ray CT).

There are numerous models for compaction of particles. [25-27] Most models neglect the release behavior and relaxation time dependence observed in nearly all pressed parts. Commonly used compaction models include: Walker - Bal'shin, Heckel, Kawakita - Ludde, and Cooper - Eaton. Varients on these compaction models include: Li et al., Ge, Panelli and Filho, Secondi, Leunberger, Shapiro, and Sonnergaard. The first 3 were applied to the UF TATB compaction data. The others are more complicated and were not evaluated. Finite element analysis of the compaction problem has been attempted by several authors. [24, 28-32] During the pressure release phase or extraction, cracks develop in the part. These have been modeled using Cam-clay[30] or Drucker-Prager approaches. [33-36] Since the cylindrical UF TATB parts did not show significant cracking, capping or delamination in X-ray CT measurements or direct observation, no effort was made to apply the fracture models.

Experimental

Most of the mold releases were kindly supplied by manufacturers and used according to manufacturer recommendation. Current practice for molding UF TATB boosters is to release the ram with talc and the die body with DC-7 silicone mold release. A wide variety of alternative mold releases are available. Several fluorocarbon telomers were evaluated. Silicones and wax based release agents were also tested. Most of the samples were aerosols, which were sprayed into the die cavity and on the upper and lower ram. No heat was required in all cases so the parts were wiped dry with Kem-Wipes and allowed to air dry for at least 1 h. Two types of Talc (spherical and platy) were tested. In this case 0.4 grams of powder was added to the die cavity with lower ram in place. The upper ram was inserted and the die shaken several minutes. The powder was emptied from the die into a dish and weighed. Residual powder remaining in the die was about 0.002 grams. Talc coatings were not especially uniform to the eye. Fluids, like DC-7 and Zyvex Flex 6, were applied with a clean soft cloth. The 12 mold releases used in this study are listed in Table 1. Ultrafine TATB from a single lot (C-122) was used in all cases. [37]

The molding procedure was as follows. After the 1.27 x 7.62 mm (1/2 x 3 inch) die body with 1.9 cm (¾") lower plunger and 5.08 cm (2") upper plunger were coated with mold release according to the manufactures recommendations, approximately 6 grams of ultrafine TATB was charged into the die body with the lower plunger inserted. The upper plunger was inserted and the explosive compacted by hand pressure. The height that the upper plunger extended above the die body was measured and the setup was transferred to an MTS 800 with Test Star II computer control. Even though TATB is an insensitive explosive, tests were conducted remotely in a closed 1.27 cm (½") steel cell. The hydraulic pressure to the test machine was initiated only when the cell was closed. A load control program compressed the plunger at 26.7 N (6 lb)/s up to 26,700 N (6000 lbf) or about 200 MPa (30,000 psi), then held this pressure for 2 minutes and then ramp down at 44.5 N (10 lb)/s until the force on the load cell was 222 N (50 lbs). The program was stopped, residual pressure released and the hydraulic power was turned off. The cell door was opened, the die was removed and the plungers extracted from the die body. A part catcher was inserted below the die and a 1.25 x 7.62 cm (½ x 3 inch) extracting plunger along with a 1.9 cm (¾ inch) rider was inserted until it contacted the top of the pressed part. The bottom of the part was marked with a sharpie pen. The die and extracting plunger were returned to the MTS with the part catcher underneath. Four cylindrical silicone pads were placed on top of the die body

to prevent contact with the extracting ram. The cell was closed, the hydraulic test machine started, and a stroke control program forced the part from the die at a rate of 0.00254 cm (0.001 in)/s while monitoring the force on the extracting plunger. A schematic of the test fixturing is shown in Figure 1.

Results

1. Compaction behavior. Prior to use of explosives, mock material is used to evaluate any new testing procedure. In this case pentaerythritol (PEY) was used because its small particle size is similar to UF-TATB. Typical loading-unloading pressure and density curves for two repeats of the PEY without mold release and one run with DC-7 silicone mold release are shown in Figure 2. The reproducibility of the two tests without mold release was excellent. The maximum calculated in-die density at 30 ksi was 1.3033 and 1.3027 gm/cc for PEY without release agent and 1.3381 with DC-7 release agent. When the pressure is released spring back occurred and the density was reduced to1.2769, 1.2771 and 1.3093 gm/cc, respectively. This is about a 2.2% improvement in density with mold release. During extraction these parts fractured and the approximate densities were 1.266 ± 0.001 gm/cc and 1.281 gm/cc with and without mold release, respectively. Most of the inter-granular packing has already occurred when the PEY was hand packed, so initially a rapid rise in density occurs by crystal aggregate packing and void filling. As the voids become fewer, crystal deformation begins to occur and the density starts to level off. [6, 38]

Compaction of Ultrafine TATB was performed using the procedures developed for the PEY mock. Results for DC-7 and two fluorocarbon spray mold releases (A-1000 and MS-122AX) are compared to TATB compaction with no mold release in Figure 3. In this case there is only about 1% improvement in density and one of the mold release agents produced lower density at 30ksi than the unreleased density. The bulk density, $\rho(0)$, of UF-TATB's was estimated from hand compaction and the height of the top plunger under no pressure, H_0. Then the density at any time, $\rho(t)$, is calculated from the position of the actuator according to Equation 1.

$$\rho(t) = w/[H_0+1.27-S(t)]\pi r^2 \qquad (1)$$

Where S(t) is the stroke movement at time t and r is the radius of the die. As the pressure is released, the sample density decreases until the pressure cycle is complete. The sample density at 300 psi, $\rho(f)$, was taken as the recovered density so the percentage of spring back, SB, was estimated from:

$$SB = (1-\rho(f)/\rho_{max}) \approx (1-\rho(part)/\rho_{max}) \approx (1-S_f/S_{max}) \qquad (2)$$

Where $\rho(part)$ is the part density after extraction, S_f is the stroke position at 1330 N (300 lbf) and S_{max} is the stroke at maximum pressure. The spring back percentages calculated in this way were between 3-4%. Table 2 gives the results from all 13 measurements for maximum density, and spring back based on Equation 2.

An alternate way of looking at the compaction curves is shown in Figure 4. Here "stress-strain curves for compaction and release are shown for neat, Flex Z6 and MS-122-AS mold released UF TATB. The strain, ε, is calculated from the stroke motion, initial length, Lo, and sample length, L, under compression or release pressure or stress, σ.

$$\sigma = P = F/A \quad (3)$$

Where P is the pressure, F is the force on the load cell and A is the area of the die.

$$\varepsilon = \Delta L/L \approx -S(t)/[H_0+1.27-S(t)] \quad (4)$$

Note that the density is related to the strain by equation 1 and is shown in the upper x-axis. Note also that the unloading trace is not linear, and therefore not simply elastic, especially near the low stress (pressure) end of the curve. This is at variance with the observations of Olinger [39] where the PBX appeared to densify during each pressure relaxation.

It is interesting to look at the rate of change of density (or stroke) as the pressure increases at a constant rate (see Figure 5). Initially the density changes very quickly with increasing pressure as the bulk UF TATB compacts to fill voids. This happens within the first minute or two of the compression cycle but only requires a pressure of 2 MPa (300 psi). Once the sample packs so that the UF TATB aggregates begin to bear significant load, the compaction rate begins to slow down and the weak aggregates begin to deform. Only early compaction and late pressure release data are shown in the figure. When most of the weak interfaces (air and aggregates) have been compressed, the crystals themselves begin to yield, flow together and adhere to each other. The figure compares NMR, Camie A1000 and Flex 6. All of the Δ(density)/Δ(time or Pressure) curves show a peak followed by rapid compaction up to about 40-50% of the maximum stroke travel (volume change). The density, however, changes only from about 1 gm/cc, from bulk density to about 1.2 gm/cc.

At maximum pressure there is a 2 minute hold during which the sample continues to densify as shown in Figure 6. There are several points of interest in this plot. First, the mold released samples that had lower extraction pressures (see below) tended to show less of an increase in density during the high pressure hold than the neat UF TATB. While the density of mold released samples which did not reduce extraction pressure increased like the neat UF TATB. This seems to imply that wall friction plays a role in this effect. Although the densities of the parts were different, indicated by different colored abscissa, the relative densities were similar. Initially, the density continues along the pressure-density trace, but within about 20-30 s changes slope and continues on until the hold cycle is finished at 2 minutes. Very shortly, within 10s, the density begins to decrease as the pressure is reduced.

Based on the final part density in Table 2, almost all of the mold releases improved the density of the part compared to neat UF TATB. The average density of all 13 tests was 1.841±0.001 g/cc.

<u>2. Extraction behavior.</u> Assuming only the radial stress and wall friction hold the part in the die; the extraction force should be constant until the part begins to exit the die. Then as the radial stress is reduced, the extraction force should change in proportion to the contact area between the material and the die. Figure 7 shows the extraction force of lubricated and neat pentaeurythritol cylinders being extracted from the die. As expected, there is a sharp rise in force until the part starts to move in the die, indicated in the figure by line “a” in 0.01 s to 10 kN (2300 lbf). This is followed by 0.02 s of slower increase, line “b”, to about 11.5 kN (2600 lbf) which remains constant (line c) until the part begins to exit the die at 1.5 cm (0.6 in) since the parts were about 2.75 cm (1.08-1.09 in) long and the lower piston was

approximately 1.27 cm (1/2”) inside the die during molding. When the part begins to exit the die at about -1.5 cm (-0.6 in) of stroke, the extraction force begins to decrease. When the actuator stops at 3.8 cm (1.5”), the part without mold release is not completely extracted and the extraction force decays from about 1200 N (275 lbf) to about 1000 N (240 lbf). The rate of decrease of extraction force is not linear with actuator motion. This has been attributed to nonuniformity of axial stress along the length of the die causing similar nonuniformity in the radial stress. [6, 8, 23]

The effect of DC-7 silicone mold release on PEY was to reduce the extraction force by about 2.7 kN (600 lbf) and the slope after exiting the die from about 4500 to 3000 N/cm (2614 to 1670 lbf/in). Also, the extraction force while the part is inside the die is different. In both cases there is an initial rapid increase in force as the part starts to move, then an increase at reduced rate to a maximum. In the sample with no mold release, this maximum extraction force was maintained; whereas in the mold released part, the extraction force dropped slowly until the part was almost at the end of the die. Both neat and mold released parts cracked at the edges on the bottom face parallel to the lower ram contact surface, see Figure 8.

The extraction behavior of UF TATB with 3 different mold releases compared to no mold release is shown in Figure 9. A factor of 5 times less force is required for UF TATB extraction compared to PEY. The same extraction characteristics are found as in PEY indicated by red lines on the neat UF TATB trace. Line “a” is the rapid rise in load required to initiate movement of the part. Once motion begins, the force required to move the part follows line “b”; slowly increasing to a maximum or inflection point. Once this point is reached, the extraction force can either level off and remaining constant, increase or decrease (line c) until the part begins to exit the die. On exiting the die (intersection of line c and d), the extraction force begins a linear decrease until the part exits the die. In some instances, for example neat UF TATB, there is an interruption in slope when about half of the part has exited the die prior to complete extraction (line e). Usually the slope increases, indicating the force to extraction a unit length of part is higher at the end of the extraction process. This is consistent with higher radial stress at the compacting ram and less at the bottom of the die. Finally when the part is out of the die, the load becomes zero or a constant (line f), indicating residual flash in the die.

The effect of mold releases on extraction of UF TATB pressed parts was much more dramatic than the compression molding traces. DC-7 silicone release agent nearly doubles the force required to initiate extraction, but the shape of the extraction curve (a, b, c, d and f) was very similar to that of neat UF TATB. After exiting the die the rate of change of load with stroke (remainder of part in the die) is almost linear throughout the extraction process and nearly parallel to line e in the neat extraction curve. The Camie A-1000 fluorocarbon release agent had nearly the same force to initiate part motion as neat UF TATB (line a) but thereafter the extraction force decreased (line b) and then increased slightly (line c) prior to the part exiting the die. After exiting the die the extraction force decreased almost linearly but with less force/unit length than the other release agents. The force required to initiate motion for Miller-Stevenson 122-AX (line a) was greater than neat UF TATB, but once motion began, the extraction force was nearly constant until the sample exited the die (lines b and c are the same). Once this part had exited the die, there are two steps in the trace (lines d and e) and the last section lies on top of the Camie fluorocarbon release agent.

The extraction curves of two other fluoropolymer release agents (MS 122 AD and Krytox) and the two different talcs are shown in Figure 10. They all require comparable or greater force to extract the UF TATB part than no mold release. They also were very similar to the trace for UF TATB without mold release as indicated by lines a-f copied from Figure 9. Note that there can be some residual force on the ram after the part has been completely extracted. Figure 11 shows the last 3 mold releases (PU, Bomb lube, and Flex 6). Flex 6 and A-1000 required the least force to extract the part. The slopes of the segments of the extraction force traces (a through e) were fitted by least squares and the results are given in Table 3.

X-ray computer tomography (X-ray CT) was performed on extracted samples 2, 3, 4, 6, 7, 9, 10 and 13 in an attempt to see what influence release agents might have on the density variation in compression molded parts. [40] Cracks were only detected in the UF TATB which used talc as the mold release (see Table 4). Since the cracks are only a few mm from the surface, this may be due to migration of the talc powder into the TATB during compaction. Since talc density is ~2.7 gm/cc, it attenuates x-rays more than TATB. Figure 12 shows X-ray CT scan of UF TATB pressed part with spherical talc (#9 – LHS) and platy talc (#10 – RHS) imbedded near the surface. The non-uniform distribution of talc (white areas in the X-ray slice) suggests it is not evenly coated over the mold surface or has moved during compaction. Why the spherical talc incorporates in the TATB more than platy talc is unknown. Comparison of the average attenuation in Table 3 with the density of the part does not show statistical correlation. Probably because of small density variations in the parts, the density distribution throughout the parts could not be resolved clearly using this technique.

Discussion

1. Loading behavior : Among the earliest methods of treating compaction curves is that of Walker and Bal'shin.[25, 27] They proposed that the density, ρ, or relative density, ρ_r, depended linearly on the log of the pressure, P:

$$\rho \text{ or } \rho_r = C_1 + k \log [P] \qquad (5)$$

where C_1 and k are constants. Early work at Pantex used the Walker dependence to fit density-pressure behavior for LX-17 compression molding data [41]. A typical plot for UF TATB without release agent and with 6 release agents is shown in Figure 13. The compaction traces are obviously not linear in log P. However, current thinking is that the initial part of the trace is associated with agglomerate rearrangement and migration controlled by interparticle friction such as can be measured by angle of repose. [19] Subsequently, once the agglomerate yield pressure is exceeded the density increases by break-up of agglomerates and crushing. The early, low pressure section stops at the agglomerate yield pressure 2 MPa (~ 300 psi). The agglomerate deformation and crushing is the most rapid densification region and is complete at the joining pressure 28 MPa (~ 4000 psi). Above the joining pressure, the densification rate slows down because it is more difficult to compress the primary particles. As can be seen in the figure, the compaction of UF TATB doesn't follow these 3 stages all that well.

When the data for compaction were replotted in terms the Heckel equation (6), only a portion of the compaction trace is relatively linear. [42] The data for UF TATB without mold release are plotted according to the Heckel relationship in Figure 14. The linear portion was from about 5000 to 30,000 psi.

$$Ln(1/(1-\rho_r)] = KP + A \quad (6)$$

The relative density, ρ_r, is taken as the calculated density ρ divided by the theoretical maximum density (TMD = 1.937 gm/cc) and P is the pressure. Obviously, this neglects densification due to increase in pressure. The linear portion (red dashed line) yields K of 8.0844E-5 $psi^{-1}$and A is 1.325. The inverse of K has been associated with the yield pressure. For UF TATB, the yield pressure is 7.83 MPa (1136 psi). This value for a yield stress in compression is not unreasonable.

Figure 15 shows the "linear" section of the Heckel plots of compaction and release for 6 different mold release agents compared to no mold release. The neat TATB data is in the middle. The "linear" region decreased as the rate of change of $ln[1/(1-\rho_r)]$ vs. P increased. Since the fits were always over the same pressure range (5000 < P < 30,000 psi), the least squares fit becomes worse as the slope increases. The relative density for primary particle deformation is obtained from the relation $D_a = 1-exp(-A)$. The fits gave yield pressures between 70 <Py<105 MPa (9-15 ksi). These values are an order of magnitude higher than the Walker and Bal'shin results. Particle deformation begins between 67 and 77% relative density. This is close to what would be expected for compaction of monomodal spheres, but higher than compaction data from pharmaceutical references. [43-47] A compilation of results for K, A, 1/K and D_a, the relative density for the onset of TATB crystal deformation are given in Table 5.

A better overall fit to the data was found for the Kawakita-Ludde equation (7). [48]

$$C= (V_o-V)/V_o = abP/(1+bP) \quad \text{or} \quad P/C = P/a + 1/ab \quad (7)$$

Where V_o and V are the initial and current part volume. P is the pressure and a and b are constants. Figure 16 shows the compaction, hold and release data for UF TATB without mold release. The fits to the compaction curve and release curve gave constants for 1/a of 2 and 2.087, respectively and 1/b of 47.5 and 4.73 MPa (6900, 686 psi), respectively. These fit pressures are associated with 50% compaction or release. The fits were quite good. Again most of the deviation occurred during the initial compaction, as can be seen by the deviation of the red trace from the dotted line fit at low pressure. Several of the very early data points were neglected to improve the compaction fit. Note that because the volume change is very small at the high pressure end, the Kawakita equation is not sensitive to density changes during the hold at 30 ksi (green points at the top of Figure 16).

Kawakita-Ludde plots for compression and decompression with 6 different mold release agents are shown in Figure 17. The compaction fit results for various mold released and neat UF TATBs are compiled in Table 6. The 50% compaction pressure (1/b) varied around 50 ± 10 MPa (7300 psi). Since for one component mixes the volume and weight percentages are equal, at the beginning of primary particle compaction according to Heckel (~70%) the Heckel yield pressure (P_y) would be around 80 MPa, consistent with 50% results using the Kawakita equation. Table 6 is a compilation of the fits for the decompression data to equation 7. The slope averaged 2.11 ± 0.1 for compaction giving a value of a = 0.47 ± 0.02. The 50% pressure was 4.8 ± 0.9 MPa (700 ± 100 psi). No attempt was made to use more complicated compaction equations because of time constraints.

2. Extraction behavior: Much less work has been done in the literature to elucidate the extraction behavior. The initial extraction segment, "a", in Figures 9-11 was fitted to equation 8 as a crude estimate of the shear modulus and strength of the sample. Here F_e is the extraction force, A is the area ($\pi r^2 = 0.196$), L_o is the length of the sample after extraction and ΔL is the change in stroke position.

$$G \approx (F_e/A)/\Delta L/L_o \qquad (8)$$

This simplistic calculation yields shear moduli around 1 GPa (± 1), see Table 3. Dynamic mechanical shear modulus measurements on dry aminated TATB at ambient were about 2 GPa. [49] Since cracking has been observed during extraction, it might also be of interest to evaluate the strength (stress) required to separate and move the molded part from the die wall. The stress at which the part separates from the wall was estimated from the intersection of line a and line b. Using this method the "strength", σ_b, required to break the part form the wall is:

$$\sigma_b = M_a(B_b-B_a)/(M_a-M_b) + B_a \qquad (9)$$

Where $M_{a,\,b}$ are the slopes of lines a and b and $B_{a,\,b}$ are the intersepts of lines a and b. The strength at the interface determined in this way varied from 6.3 to 15 MPa (920 to 2100 psi). Only release agents #3 and 13 had lower strengths than the unreleased UF TATB.

Once the sample has separated from the die wall, the extraction force, F_e, should be controlled by the residual radial stress, σ_r, from the compaction process and the dynamic coefficient of friction, μ, between the part and die surface. The simplest result would be be:

$$\mu = F_r/ F_e = \sigma_r/P_e \qquad (10)$$

Unfortunately only release agents #3, 4, 5, and 12 had reasonable constant extraction forces. In most of the others (1, 2, 6, 7, 8, 9, 10 and 13), the extraction force seemed to increase until the part exited the die. Only #11 decreased continuously while the part approached the end of the die. If the average extraction force before the part exits the die and the coefficient of friction for LX-17-1 at ambient against stainless steel (0.17 ±0.01) [50] are used in equation 10 from UF TATB without mold release, the average radial force in the die would be 7064 N (1588 lbf).

No attempt was made to evaluate capping or delamination behavior or density distributions because these effects were not observed in UF TATB either by X-ray CT or directly by eye. It may be possible to determine under what conditions capping and delamination could occur.

Conclusions

Twelve different mold releases were evaluated for their effectiveness on compaction and extraction of right circular cylinders of UF TATB. The compaction and pressure release traces were all very similar, indicating that the release agent had minimal effect on molding the part. The densification during the hold segment of compaction tended to correlate with the ease of extraction. The extraction force required to remove the molded part varied from 800 to 2.1 kN (180 to 480 lbf). The release agents could be grouped into 3 categories based on the force required to extract the part. Category 1 required

about the same extraction force as untreated UFTATB, 2. Category 2 required higher extraction force and category 3 Lower extraction force. The shape of the extraction curves varied also. Only three were nearly constant as the part moved toward the end of the die, as expected if kinetic wall friction alone controlled the extraction process. Most showed increasing force as the part moved toward the end of the die but one showed a dramatic decrease in force after the part began to move. Camie-Campbell A-1000, a fluorocarbon spray release agent, required the least force to extract the part in these tests.

Three models were fitted to the compaction and release curves. Walker-Bas'hin fits appear to have 3 stages, but did not separate the release agents clearly. Heckel fits over the linear compaction range gave yield pressures for the UF TATB particles between 70-105 MPa. One would expect these values to be similar since all of the UF TATB is from the same lot of material. These values do not seem to correlate with the extraction results for various release agents. There was a significant curvature in the Heckel plots for the different mold releases, but this also did not correlate with extraction results. Kawakita fits also differed with different release agents but did not correlate with extraction results. The Kawakita plots could be fitted over the entire compaction or release section of the data except for the very early section where the data has significant scatter and the compaction method may be different.

The density distribution within a part continues to be elusive. The source of the problem appears to be two fold. First, the density may be fairly uniform. Second, the x-ray energy may be too high. Some effort is continuing in this area.

Suggestions for Future work:

It would be useful to improve the instrumentation in the die. Load cells on the die and at the lower ram would help identify friction and load losses. An extensometer to follow the upper ram motion would also be useful. Temperature capability on the die will be needed for explosives with binder. Finally multiple cycle capability should be programmed and evaluated.

Other explosives would be interesting to evaluate. Detonator explosives like LLM-105, HNS, and PETN could be evaluated. Binder formulations such as PBX 9407, LX-16 and LX-18 would be of interest if temperature and multiple cycles were available. Main charge PBXs and their precursor explosives could be evaluated as well. Neither compaction nor extraction rate dependence was investigated.

Investigation of capping, delamination and cracking using Cam-Clay or Drucker-Prager models could be evaluated. Time dependent models for densification during pressure holds and unrelaxed dwells during multiple cycling should be developed. Tools for characterization of the part density distributions should be investigated and developed.

Acknowledgements:

We wish to acknowledge several people who supported this effort. Ken Morales and Dan Schneberk ran and analyzed the X-ray CT. Thomas Lorenz helped run the MTS equipment. Franco Gagliardi and Sally Weber kept track of sample shipments and provided insight into pressing of explosives. Trevor Wiley provided input for the X-ray CT work and ran samples at the synchrotron

source in Berkeley. George Overture also provided useful insight into various aspects of detonator production. Special thanks to Lennon Mings for his interest and elucidation of the production process at Pantex.

References

1. T. A. Ring, *Fundamentals of Ceramic Powder Processing and Synthesis*, in *Ch 13.5.3 - Stress Distribution in the Ceramic Compact*. 1996, Academic Press: San Diego, CA. p. 661-670.
2. P. R. Mort, R. Sabia, D. E. Niesz, and R. E. Riman, *Automated generation and analysis of powder compaction diagrams,* Powder Technology, 1994, **79**, 111-119.
3. S.-T. Hong, Y. Hovanski, C. A. Lavender, and K. S. Weil, *Investigation of Die Stress Profiles During Powder Compaction Using Instrumented Die,* Journal of Materials Engineering and Performance, 2008 **17**(3), 382-386.
4. G. Jiang, G. S. Daehn, J. J. Lannutti, Y. Fu, and R. H. Wagoner, *Effects of Lubrication and Aspect Ratio on the Consolidation of Metal Matrix Composites under Cyclic Pressure,* Acta Meterialia, 2001, **49**, 1471-1477.
5. L. Seton, M. Roberts, and F. Ur-Rehman, *Compaction of recrystallised ibuprofen,* Chemical Engineering Journal, 2010, **164**(2-3), 449-452.
6. C. D. Ellison, B. J. Ennisb, M. L. Hamada, and R. C. Lyon, *Measuring the distribution of density and tabletting force in pharmaceutical tablets by chemical imaging,* Journal of Pharmaceutical and Biomedical Analysis, 2008, **48** 1-7.
7. P. V. Marshall, P. York, and J. Q. Maclaine, *An investigation of the effect of the punch velocity on the compaction properties of ibuprofen,* Powder Technology, 1993, **74** 171-177.
8. P. R. Laity and R. E. Cameron, *A small-angle X-ray scattering study of powder compaction,* Powder Technology 2008, **188**, 119-127.
9. A. B. Bashaiwoldu, F. Podczeck, and J. M. Newton, *A study on the effect of drying techniques on the mechanical properties of pellets and compacted pellets,* European Journal of Pharmaceutical Sciences, 2004, **21**, 119-129.
10. B. Azhdara, B. Stenberga, and L. Kari, *Determination of dynamic and sliding friction, and observation of stick-slip phenomenon on compacted polymer powders during high-velocity compaction,* Polymer Testing 2006, **25**, 1069-1080.
11. B. Azhdara, B. Stenberga, and L. Kari, *Determination of springback gradient in the die on compacted polymer powders during high-velocity compaction,* Polymer Testing 2006, **25**, 114-123.
12. P. Shivanand and O. L. Sprockel, *Compaction behavior of cellulose polymers,* Powder Technology, 1992, **69**, 177-184.
13. M. Li, M. Huang, B. Kang, M. P. Wen, H. Z. Li, and R. Xu, *Quality evaluation of RDX crystalline particles by confined quasi-static compression method,* Propellants Explosives Pyrotechnics, 2007, **32**(5), 401-405.
14. W. L. Elban and M. A. Chiarito, *Quasi-Static Compaction Study of Coarse HMX Explosive,* Powder Technology, 1986, **46** 181 - 193.
15. H. W. Sandusky and W. L. Elban, *Quasi-static compaction of porous propellant beds. II. Experiments and application of lattice compaction model to cannon propellants,* Powder Technology 1996, **89**, 219-229.
16. N. Kaliyan and R. V. Morey, *Constitutive model for densification of corn stover and switchgrass,* Biosystems Engineering 2009, **104**, 47-63.
17. D. M. R. Georget, R. Parker, and A. C. Smith, *A study of the effects of water content on the compaction behaviour of breakfast cereal flakes,* Powder Technology 1994, **81**, 189-195.

18. Y. Li, H. Liu, and A. Rockabrand, *Wall friction and lubrication during compaction of coal logs,* Powder Technology, 1996, **87** 259-267.
19. B. J. Briscoe and S. L. Rough, *The effects of wall friction in powder compaction,* Colloids and Surfaces SURFACES A: Physicochemical and Engineering Aspects, 1998, **137** 103-116.
20. D. E. Hare, D. R. Goosman, K. T. Lorenz, and E. L. Lee, *Application of the Embedded Fiber Optic Probe in High Explosive Detonation Studies: PBX 9502 and LX-17.*, in *13th International Detonation Symposium*. 2006: Norfolk, VA,.
21. M. H. Keshavarz, *A simple approach for determining detonation velocity of high explosive at any loading density,* Journal of Hazardous Materials, 2005, **A121**, 31-36.
22. P. C. Souers, R. L. Druce, J. Roeske, Franklin , P. Vitello, and C. May, *A Complete Detonator, Booster, and Main Charge Study of LX-07/PBX 9502,* Propellants Explosives and Pyrotechnics, 2011, **36**, 119 - 124.
23. A. Djemai and I. C. Sink, *NMR imaging of density distributions in tablets,* International Journal of Pharmaceutics, 2006, **319**, 55-62.
24. C.-Y. Wu, B. C. Hancock, A. Mills, A. C. Bentham, S. M. Best, and J. A. Elliott, *Numerical and experimental investigation of capping mechanisms during pharmaceutical tablet compaction,* Powder Technology, 2008, **181** 121-129.
25. P. J. Denny, *Compaction equations: a comparison of the Heckel and Kawakita equations,* Powder Technology 2002, **127** 162- 172.
26. J. M. Montes, F. G. Cuevas, J. Cintas, and Y. Torres, *Powder compaction law for cold die pressing,* Granular Matter, 2010, **12**, 617-627.
27. T. Çomoğlu, *An Overview of Compaction Equations,* J. Fac. Pharm, Ankara, 2007, **36**(2), 123 - 133.
28. J. D. Prigge and K. Sommer, *Numerical Investigation of Stress Distribution during Die Compaction of Food Powders,* Particulate Science and Technology, 2011, **29**(1), 40-52.
29. D. C. Andersson, P.-L. Larsson, A. Cadario, and P. Lindskog, *On the influence from punch geometry on the stress distribution at powder compaction,* Powder Technology 2010, **202**, 78-88.
30. M. A. Tripodi, V. M. Puri, H. B. Manbeck, and G. L. Messing, *Elastoplastic finite element model development and validation for low pressure uniaxial compaction of dry cohesive powders,* Powder Technology 1995 **85**, 241-251.
31. N. Zahlan, D. T. Knight, A. Backhouse, and G. A. Leiper, *Modelling powder compaction and pressure cycling,* Powder Technology, 2001, **114** 112-117.
32. I. M. Cameron and D. T. Gethin, *Exploration of die wall friction for powder compaction using a discrete finite element modelling technique,* Modelling Simul. Mater. Sci. Eng. () 2001, **9**, 289-307.
33. J. A. Hernandez, J. Oliver, J. C. Cante, and R. Weyler, *Numerical modeling of crack formation in powder forming processes,* International Journal of Solids and Structures, 2011, **48**(2), 292-316.
34. L. H. Han, E. J.A., B. A.C., A. Mills, G. E. Amidon, and B. C. Hancock, *A modified Drucker-Prager Cap model for die compaction simulation of pharmaceutical powders,* International Journal of Solids and Structures 2008, **45**, 3088-3106.
35. A. Michrafy, D. Ringenbacher, and P. Tchoreloff, *Modelling the compaction behaviour of powders: application to pharmaceutical powders,* Powder Technology 2002, **127** 257- 266.
36. T. Sinha, J. S. Curtis, B. C. Hancock, and C. Wassgren, *A study on the sensitivity of Drucker–Prager Cap model parameters during the decompression phase of powder compaction simulations,* Powder Technology 2010, **198**, 315-324.
37. P. K. Tang. *High Explosive model and its application to booster performance*. in *3rd International Symposium on High Dynamic Pressures*. 1989. La Grande Motte, France.

38. N. S. Wood, *Compact coherency and the classification of compactableand non-compactable materials from compression/compaction curves,* Advanced Powder Technol, 1993, **4**(4), 241-253.
39. B. Olinger, *Compacting PBX Molding Powders to Dense Solids*, M. ESA-WMM-03-077, Editor. Oct. 22, 2003, Los Alamos National Lab. p. 1-16.
40. D. Schneberk, T. Willey, M. Gresshoff, and K. Morales, *CT of HE Pellets – B191 System*, in *unpublished results*. 2011.
41. J. D. Harrell, *A Study of the Compaction Process for TATB Formulations*, DOE, Editor. 1980, Mason & Hanger - Silas Mason Co, Inc. Pantex Plant. p. 1-9.
42. W. Heckel, *An analysis of powder compaction phenomena,* Trans. Metall. Soc AIME 1961, **221**, 671-675.
43. O. A. Adetunji, M. A. Odeniyi, and O. A. Itiola, *Compression, Mechanical and Release Properties of Chloroquine Phosphate Tablets containing corn and Trifoliate Yam Starches as Binders,* Tropical Journal of Pharmaceutical Research, 2006, **5**(2), 589-596.
44. A. B. Bashaiwoldu, F. Podczeck, and J. M. Newton, *Compaction of and drug release from coated pellets of different mechanical properties,* Advanced Powder Technology, 2010.
45. E. Martins, I. Christiana, and K. Olobayo, *Effect of Grewia gum on the mechanical properties of Paracetamol tablet formulations,* African Journal of Pharmacy and Pharmacology, 2008, **2**, 1-6.
46. A. Okunlola and O. A. Odeku, *COMPRESSIONAL CHARACTERISTICS AND TABLETING PROPERTIES OF STARCHES OBTAINED FROM FOUR DIOSCOREA SPECIES,* Farmacia 2009, **57**(6), 756-770.
47. Y. Zhang, Y. Law, and S. Chakrabarti, *Physical Properties and Compact Analysis of Commonly Used Direct Compression Binders,* AAPS Pharm Sci Tech, 2003, **4**(4).
48. K. Kawakita and K. H. Ludde, *Some considerations on powder compaction equations,* Powder Technology, 1970/71, **4**, 61-68.
49. D. M. Hoffman, *Dynamic Mechanical Signatures of Aged LX-17-1 Plastic Bonded Explosive,* Journal of Energetic Materials, 2001, **19**, 163-193.
50. D. M. Hoffman and J. B. Chandler, *Some Aspects of the Tribology of the LX-17-1, an Insensitive High Explosive, UCRL-JRNL-205201*. 2004, Lawrence Livermore National Laboratory, Livermore, CA 94550. p. 1-21.

This work performed under the auspices of the U.S. Department of Energy by Lawrence Livermore National Laboratory under Contract DE-AC52-07NA27344.

Table 1. Mold releases and resulting densities of parts pressed to 30,000 psi

Test #	Mold release	Type	Density† (gm/cc)	Measured (gm/cc)	Manufacturer
1	none		1.8333	1.8376	
2	DC7	Silicone	1.8532	1.8406	Dow Corning
3	Camie 1000	Oligomer fluorocarbon	1.8427	1.8410	Camie-Campbell, Inc
4	MS 122AX	Oligomer fluorocarbon	1.8334	1.8393	Miller-Stephenson
5	Eject-it E28	Fluorofilm Dry Coat	1.8272	1.8427	Price-Driscoll Corp
6	MS122AD	Oligomer fluorocarbon	1.8458	1.8420	Miller-Stephenson
7	MS122DF*	Oligomer fluorocarbon	1.8466	1.8406	Miller-Stephenson
8	Krytox	Oligomer fluorocarbon	1.8431	1.8448	IMS
9	S-202	Spherical Talc	1.8536	1.8420	Silverline
10	N-99	Platy Talc	1.8283	1.8451	Nytal
11	Premium U/PAR	Paintable mold release	1.8183	1.8402	Price-Driscoll
12	UltraII sili	Silicone	1.8179	1.8386	Price-Driscoll
13	Zyvex Flex-6	3 part Wax treatment	1.8222	1.8423	Zyvex, Inc
		Average	1.836	1.842	
		Standard Deviation	0.013	0.002	

* No longer commercially available. ‡ Density estimated from end of pressing run (~300 psi in die).
† Average of three measurements.

Table 2. Properties of compacted and uncompacted UF TATB.

ID	ρ(bulk)†	ρ(30ksi t=0)	Δρ (hold)*	ρ (max)	SB(%)	Δρ(SB)
1	0.984	1.8964	0.0036	1.9	3.28%	0.067
2	1.06	1.9173	0.0042	1.9215	4.14%	0.068
3	0.998	1.9055	0.0038	1.9093	3.52%	0.067
4	1.015	1.895	0.0036	1.8986	2.74%	0.065
5	1.047	1.8884	0.0033	1.8917	2.55%	0.065
6	0.938	1.9097	0.0037	1.9134	3.24%	0.068
7	0.979	1.9082	0.0035	1.9117	3.23%	0.065
8	1.042	1.9028	0.0036	1.9064	3.12%	0.063
9	0.980	1.9167	0.0039	1.9206	3.76%	0.067
10	1.069	1.8884	0.0035	1.8919	2.27%	0.064
11	0.916	1.8759	0.0049	1.8808	1.57%	0.063
12	0.961	1.8758	0.0047	1.8805	1.86%	0.063
13	1.007	1.8814	0.0036	1.885	2.71%	0.063
Ave	1.000	1.897	0.0038	1.901	2.92%	0.065
stdev	0.047	0.014	0.0005	0.014	0.74%	0.002

*- measured density after extraction

† - based on Ho in the die without pressure

Table 3. Extraction behavior for different mold releases –fits to lines a-3 for Figures 9-11.

Test #	shear modulus (a) (GPa/psi)	σ_b MPa (psi)	line b MPa (psi)	line c MPa (psi)	Coefficient of friction	line d MPa (psi)	line e MPa (psi)
1	1.00 (1.45 E5)	6.85 (993)	13.0 (1890.1)	6.95 (1010)	0.17	-8.18 (-1190)	-13.3 (-1930)
2	2.46 (3.57 E5)	13.2 (1900)	22.8 (3314)	3.75 (544.4)	0.283	-1.69 (-2448)	no change
3	1.67 (2.42 E5)	6.37 (924)	-1.05 (-152.06)	1.95 (282.7)	0.128	-6.38 (-925.3)	no change
4	2.28 (3.31 E5)	8.94 (1300)	8.76 (1270)	8.76 (1270)*	0.128	-9.31 (-1350)	no change
5	3.01 (4.36 E5)	8.98 (1300)	8.53 (1240)	8.55 (1.240)*	0.152	-8.82 (-1279)	no change
6	1.38 (2.00 E5)	6.98 (1000)	14.2 (2005)	5.75 (833)	0.196	-12.2 (-1760)	-15.4 (-2239)
7	2.41 (3.50 E5)	8.33 (1200)	-7.01 (-1017)	6.43 (931.9)	0.157	-12.0 (-1735)	-7.18 (-1040)
8	3.19 (4.63 E5)	9.55 (980)	-9.27 (-1344)	5.75 (833.8)	0.164	-11.1 (-1608)	no change
9	1.72 (2.49 E5)	8.27 (1200)	0	7.00 (1015)	0.170	-12.1 (-1759)	-5.50 (-789)
10	1.52 (2.21 E5)	6.77 (980)	16.2 (2345.6)	11.2 (1.620)	0.189	-14.0 (-2031)	weak change
11	2.63 (3.82 E5)	14.9 (2160)	0	4.75 (688)	0.164	-13.2 (-1912)	-4.10 (-595)
12	4.43 (6.42 E5)	12.1 (1750)	7.57 (1098)	7.57 (1098)*	0.22	-13.1 (-1903)	-9.06 (-1315)
13	9.66 (1.40 E5)	6.38 (925)	0	4.82 (699)	0.132	-9.07 (-1315)	-9.62 (-1395)
Ave	1.013 (3.2 E5)	9.0 (1310)		6.40 (928)	0.173	-11.3 (-1630)	-9.2 (1330)
sd	0.98 (1.4 E5)	2..7 (400)		2.4 (345)	0.04	2.8 (400)	4.1 (590)

*this section is linear – no slope only averaged pressure as if constant friction coefficient.

Green test # indicates samples which were x-rayed.

Table 4 – Summary Statistics and Results from X-ray Scanning

Mold release	Average (St. Dev)	Cracks	Voids
DC-7 (#2)	0.100489 (0.006641)	None detected	2
A-1000 (#3)	0.100415 (0.006376)	None detected	1
MS 122AX (#4)	0.100923 (0.007822)	None detected	4
MS 122AD (#6)	0.100382 (0.006516)	None detected	1
MS 122 DF (#7)	0.100305 (0.006655)	None detected	5
N-99 Platy (#9)	0.100584 (0.00664)	2 detected – 0.5 mm in depth	8
S-202 sph (#10)	0.100625 (0.00651)	1 detected – 2 mm in depth	0
Zyvex Flex-6 (#13)	0.100788 (0.007467)	None detected	1

Table 5. Fit parameters for the linear portion of the Heckel plots of compaction curves for various mold released UF TATB samples are given below.

Mold	**A**	**K**	**ln A**	**1/K=Py**	**Py**	**Da**	
ID #		1/psi		psi	MPa	%	R^2
1	3.763	8.08E-05	1.325217	1.24E+04	85.29	73.43%	0.999
2	3.4535	9.88E-05	1.239388	1.01E+04	69.79	71.04%	0.955897
3	3.6135	8.86E-05	1.284677	1.13E+04	77.84	72.33%	0.990423
4	3.8208	8.02E-05	1.34046	1.25E+04	86.00	73.83%	0.9987
5	4.1248	7.34E-05	1.417018	1.36E+04	93.96	75.76%	0.99937
6	3.3697	9.46E-05	1.214824	1.06E+04	72.91	70.32%	0.9933
7	3.5733	9.09E-05	1.27349	1.10E+04	75.81	72.01%	0.99254
8	3.9422	8.41E-05	1.371739	1.19E+04	81.95	74.63%	0.99663
9	3.1683	1.02E-04	1.153195	9.78E+03	67.42	68.44%	0.9725
10	3.9096	7.56E-05	1.363435	1.32E+04	91.18	74.42%	0.9995
11	4.318	6.59E-05	1.462792	1.52E+04	104.60	76.84%	0.99791
12	4.1502	6.63E-05	1.423157	1.51E+04	104.03	75.90%	0.9991
13	3.9719	7.07E-05	1.379245	1.41E+04	97.48	74.82%	0.9998
Ave	3.782985	8.25E-05	1.326818	12364.49	85.25072	0.733676	0.991898
Std Dev	0.335002	1.2E-05	0.089978	1801.934	12.42397	0.024349	0.013102

Table 6. Fit parameters for the Kawakita-Ludde plots of compaction curves for various mold released UF TATB samples are given below. Mold release agents ID numbers are given in Table 1.

ID #	Slope	intercept	a=1/slope	b=1/(a/intercept)		r^2 of fit
				psi	MPa	
1	2.0026	3418	0.499351	6844.887	47.19	0.99956
2	2.1209	4268.9	0.471498	9053.91	62.42	0.99969
3	2.0023	3437.9	0.499426	6883.707	47.46	0.99963
4	2.0492	3839.8	0.487995	7868.518	54.25	0.99971
5	2.1226	4153.7	0.47112	8816.644	60.79	0.99978
6	1.9036	2941	0.52532	5598.488	38.60	0.9996
7	1.9614	3208.7	0.50984	6293.544	43.39	0.99969
8	2.0965	4034.5	0.476985	8458.329	58.32	0.99986
9	1.9644	3320.6	0.509061	6522.987	44.97	0.9996
10	2.1445	4484.3	0.466309	9616.581	66.30	0.9996
11	1.8823	2602.5	0.531265	4898.686	33.78	0.99986
12	1.9659	2997	0.508673	5891.802	40.62	0.99965
13	2.0535	3814.7	0.486973	7833.486	54.01	0.99964
Ave	2.020746	3578.585	0.495678	7275.505	50.16315	0.999682
Std Dev	0.084954	570.5189	0.020928	1452.765	10.01652	9.77E-05

Table 7. Fit parameters for the Kawakita-Ludde plots of pressure release curves for various mold released UF TATB samples are given below. Mold release agents ID numbers are given in Table 1.

ID #	Slope	intercept	a=1/slope	b=a*intercept		r^2 of fit
				psi	MPa	
1	2.087	323.43	0.4792	675	4.65	0.99997
2	2.229	389.85	0.4487	869	5.99	0.99997
3	2.089	318.73	0.4788	666	4.59	0.99997
4	2.149	348.73	0.4653	749	5.17	0.99997
5	2.230	392.27	0.4484	874	6.03	0.99996
6	1.977	281.85	0.5057	557	3.84	0.99998
7	2.042	296.66	0.48969	605	4.18	0.99998
8	2.203	372.42	0.45401	820	5.66	0.99997
9	2.047	305.2	0.4885	624	4.31	0.99997
10	2.262	402.12	0.4421	910	6.27	0.99996
11	1.947	251.64	0.5136	490	3.38	0.99998
12	2.036	274.62	0.4910	559	3.86	0.99998
13	2.15	336.86	0.4651	724	4.99	0.99997
Ave	2.111	330.3	0.4746	702	4.84	0.999972
Std Dev	0.101	48.5	0.0227	135	0.94	6.89E-06

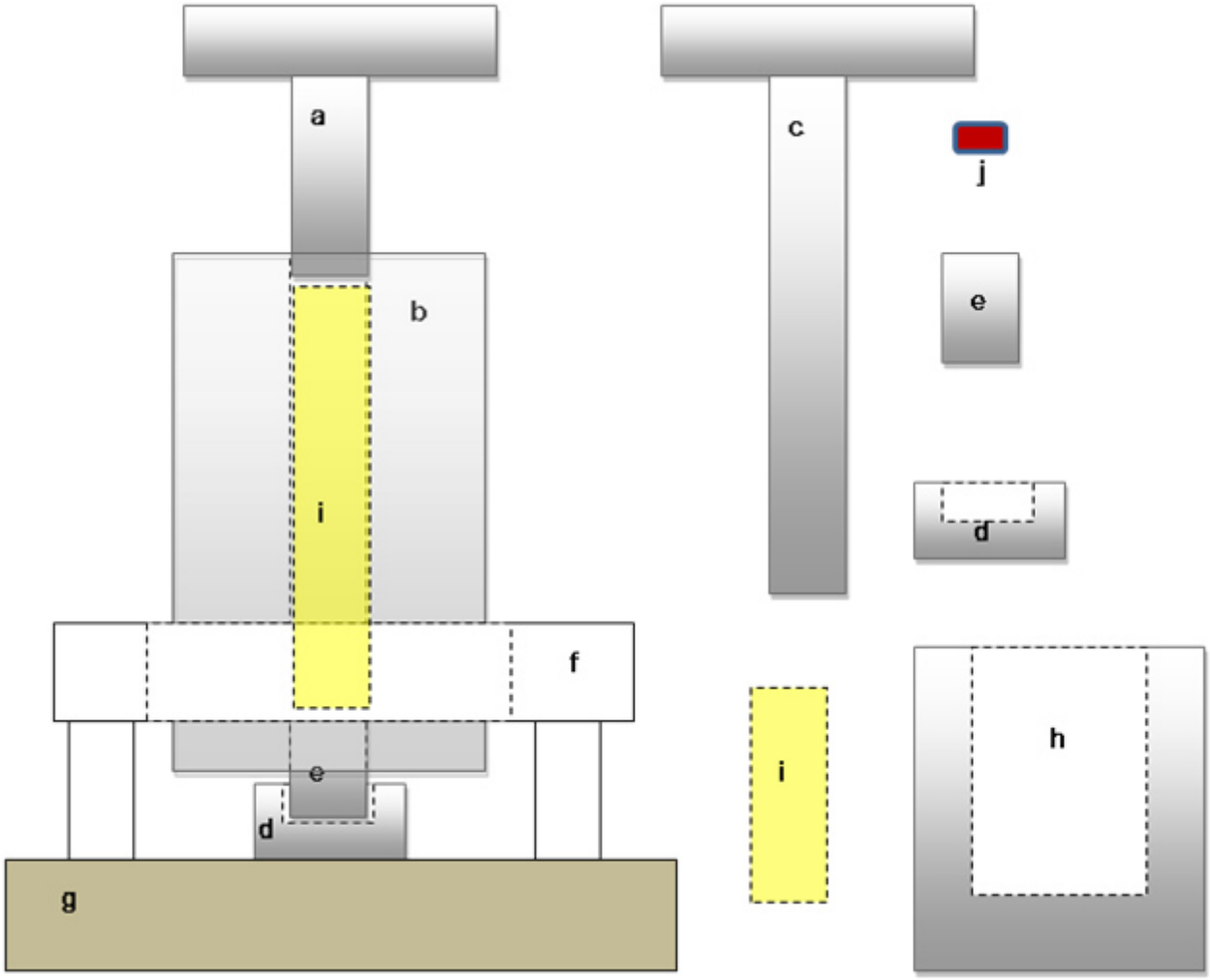

Figure 1. : Parts and test set up for compression molding in MTS include: (a). 2” molding ram; (b). 3” die body; (c). 3” extractor ram; (d). bottom button; (e). ¾” bottom ram; (f). ring fixture for holding die; (g). bottom platen attached to MTS actuator; (h). catcher and (i). Powder or molded part. Three of four small rubber buttons (j) were used in the extraction process to prevent complete closure of the extraction ram.

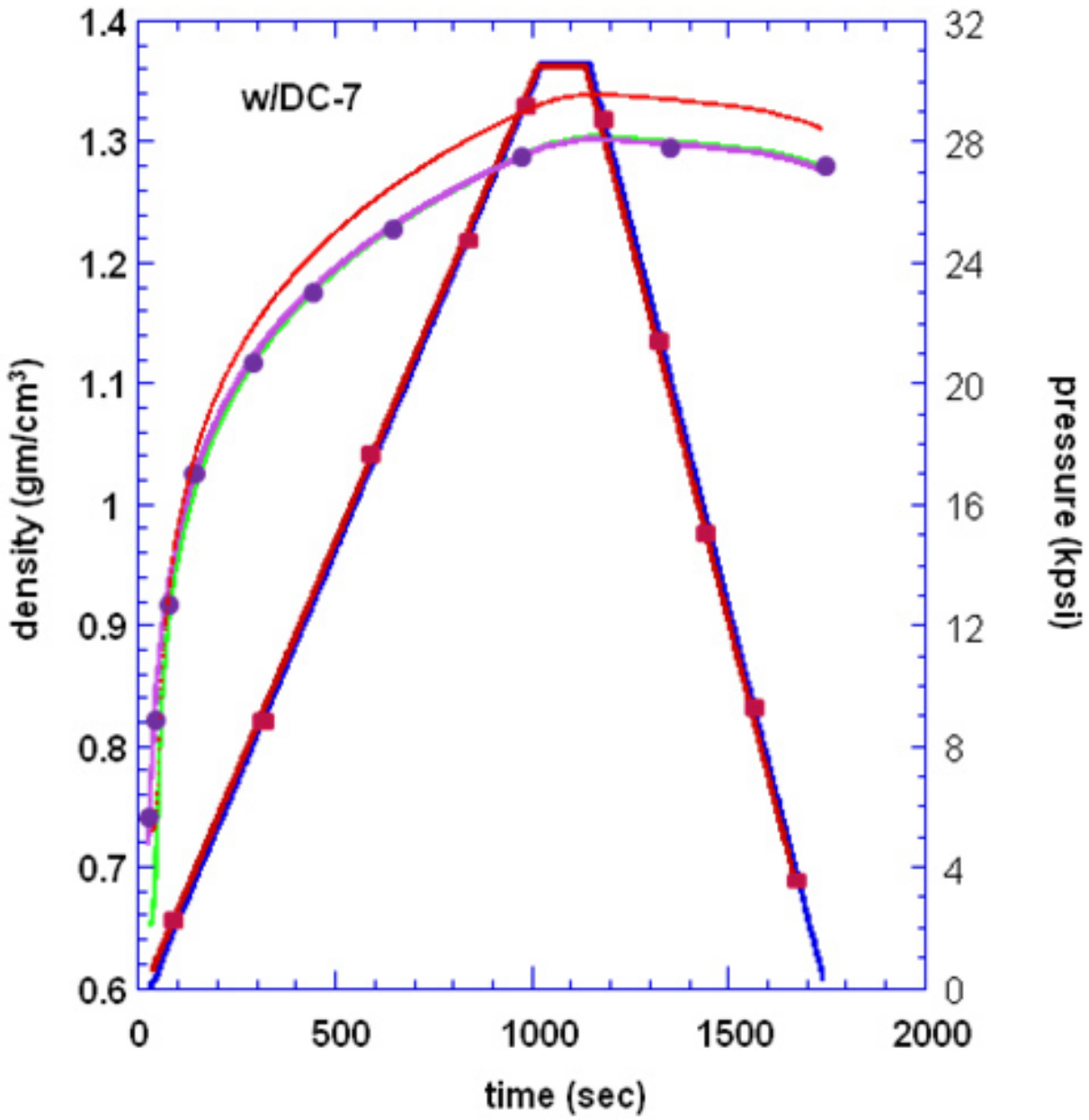

Figure 2, Density and pressure versus time traces for compaction of pentaerythritol show improved in-die density using DC-7 silicone mold release (red traces). Densities of the extracted parts were about 1.266 for both parts without mold release compared to 1.281 gm/cc with mold release.

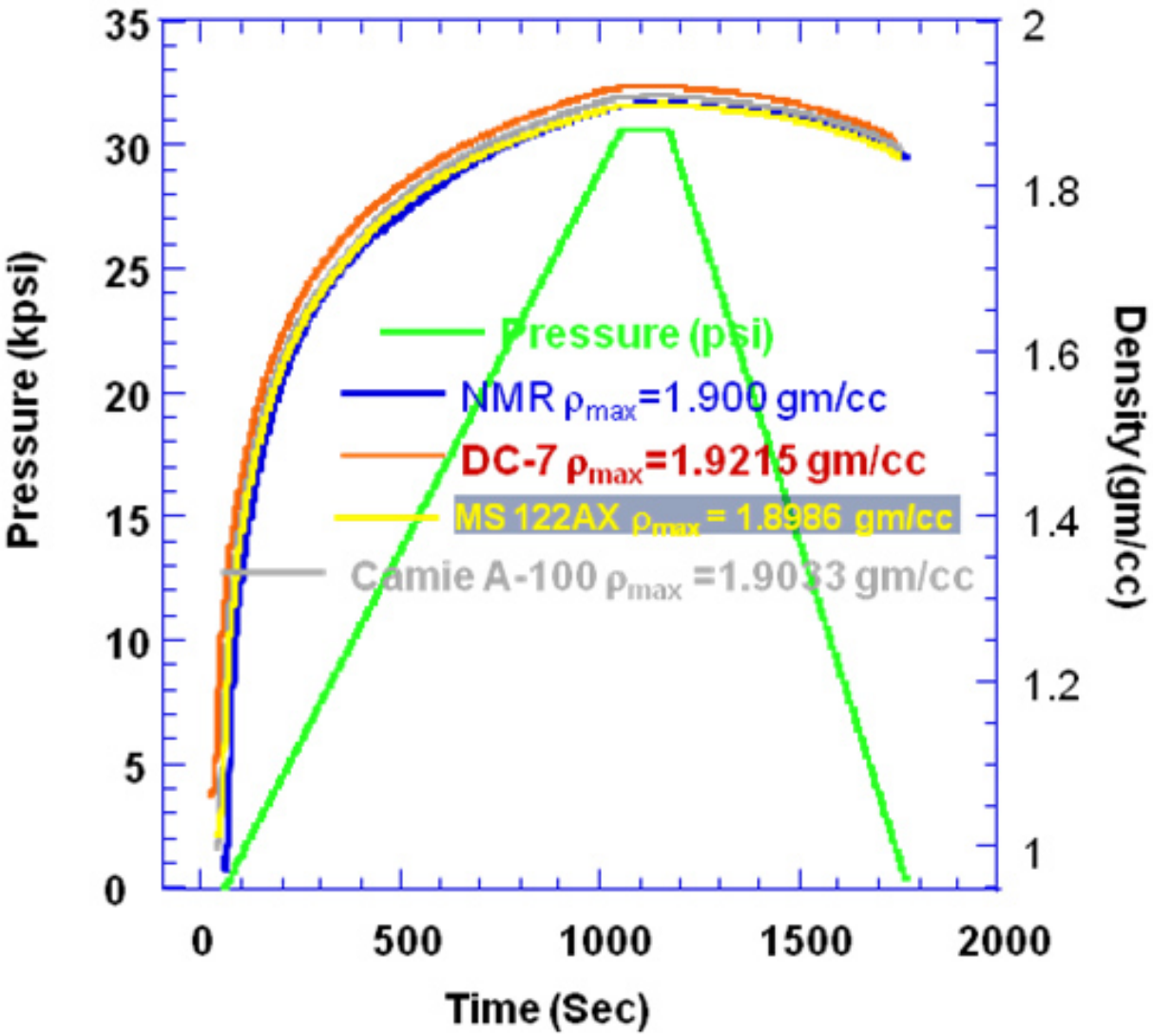

Figure 3. Compaction of neat UF TATB lot C-122 and with several different mold release agent showed much less difference than PEY in Figure 2.

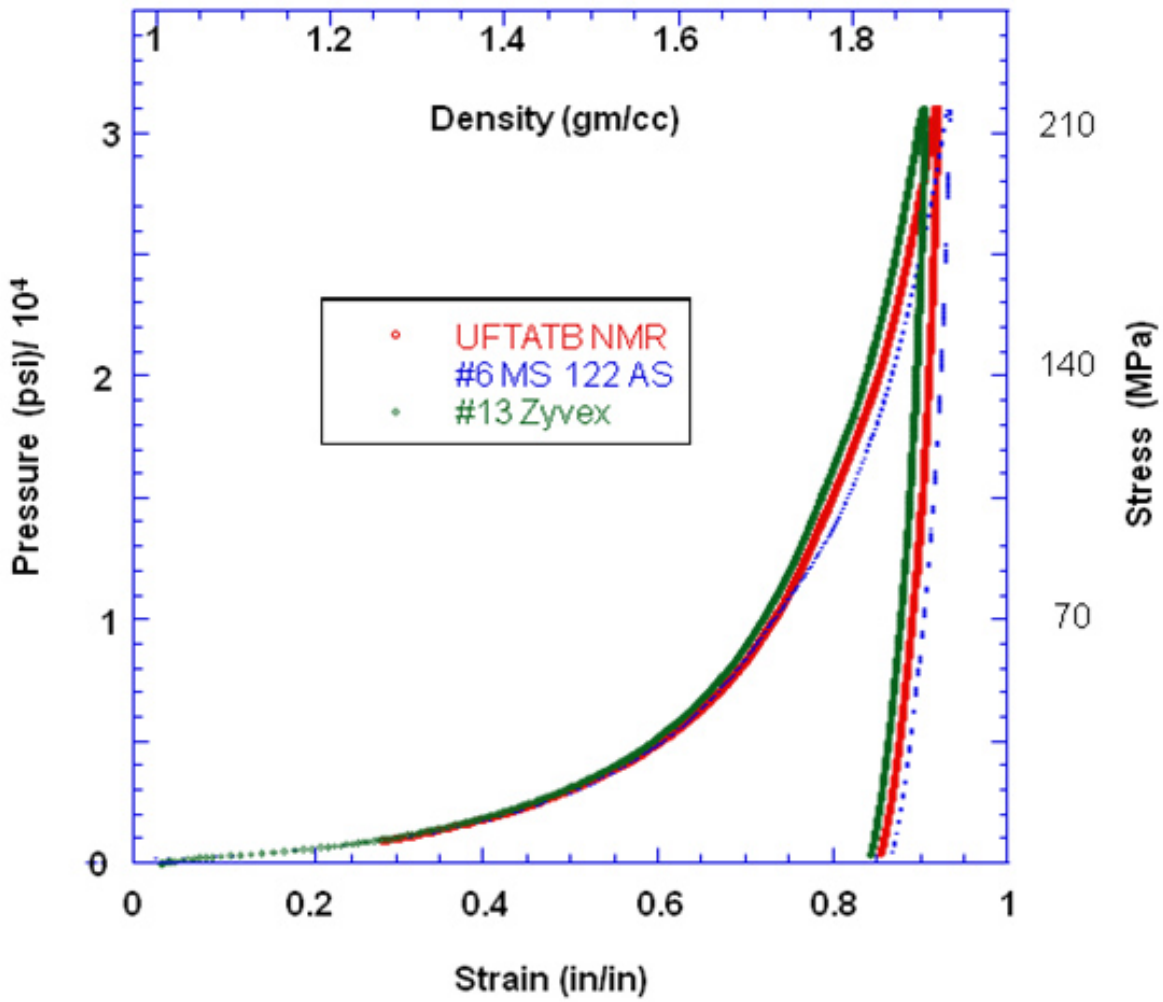

Figure 4. The pressure-density trace is equivalent to a stress strain plot showing the compaction of the part and recovery as the pressure is released. Only small differences were observed with various types of mold releases. Note that the release curve is not linear, so the compact part decompression is not elastic.

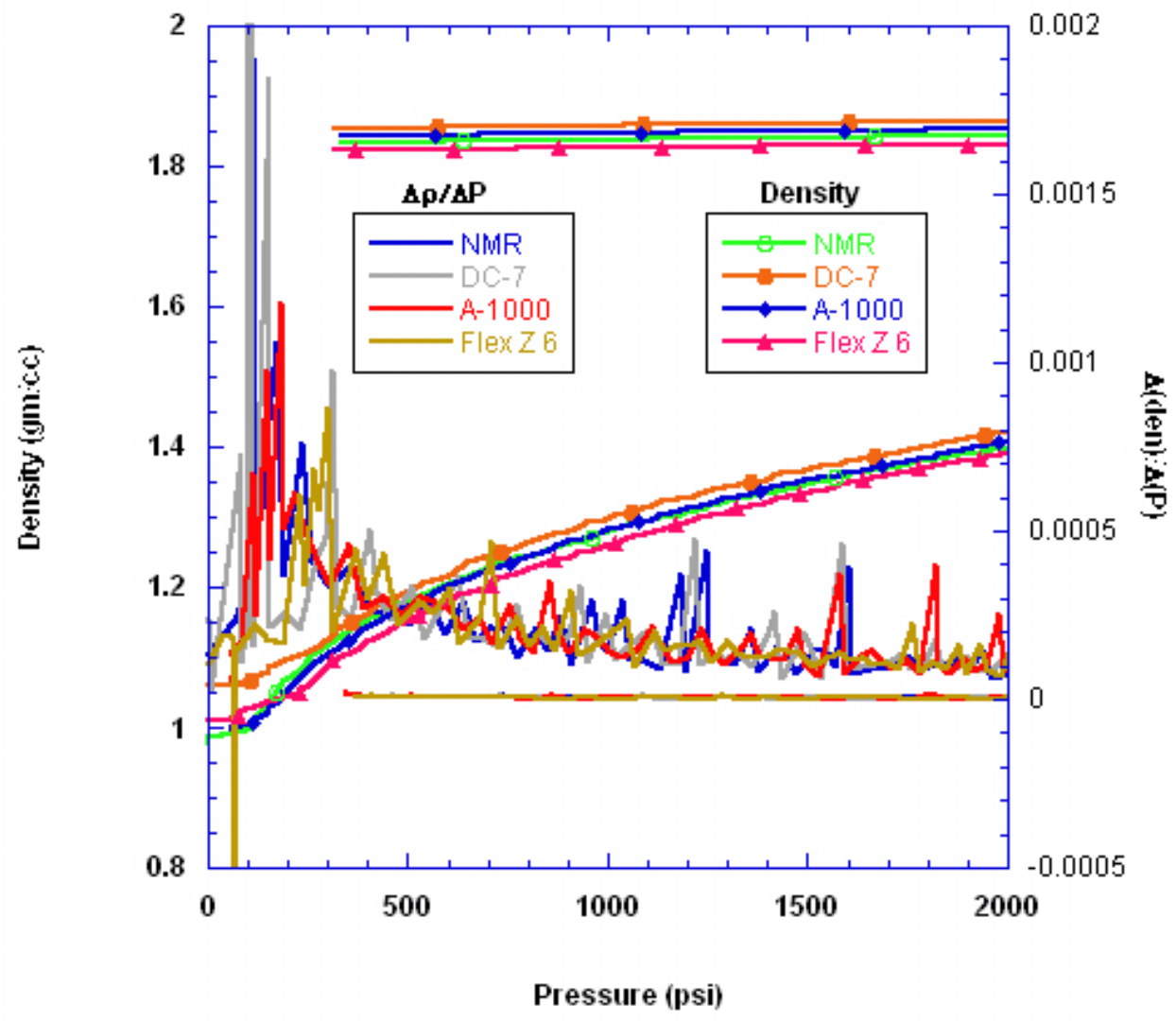

Figure 5. As the density increases within the first minute of compaction, the rate of densification with pressure goes through a maximum because the TATB powder flows rapidly to fill voids. Slower compaction follows as aggregate particles start to compress at relatively low pressures. Only early compaction and late pressure release (almost straight lines) curves are shown.

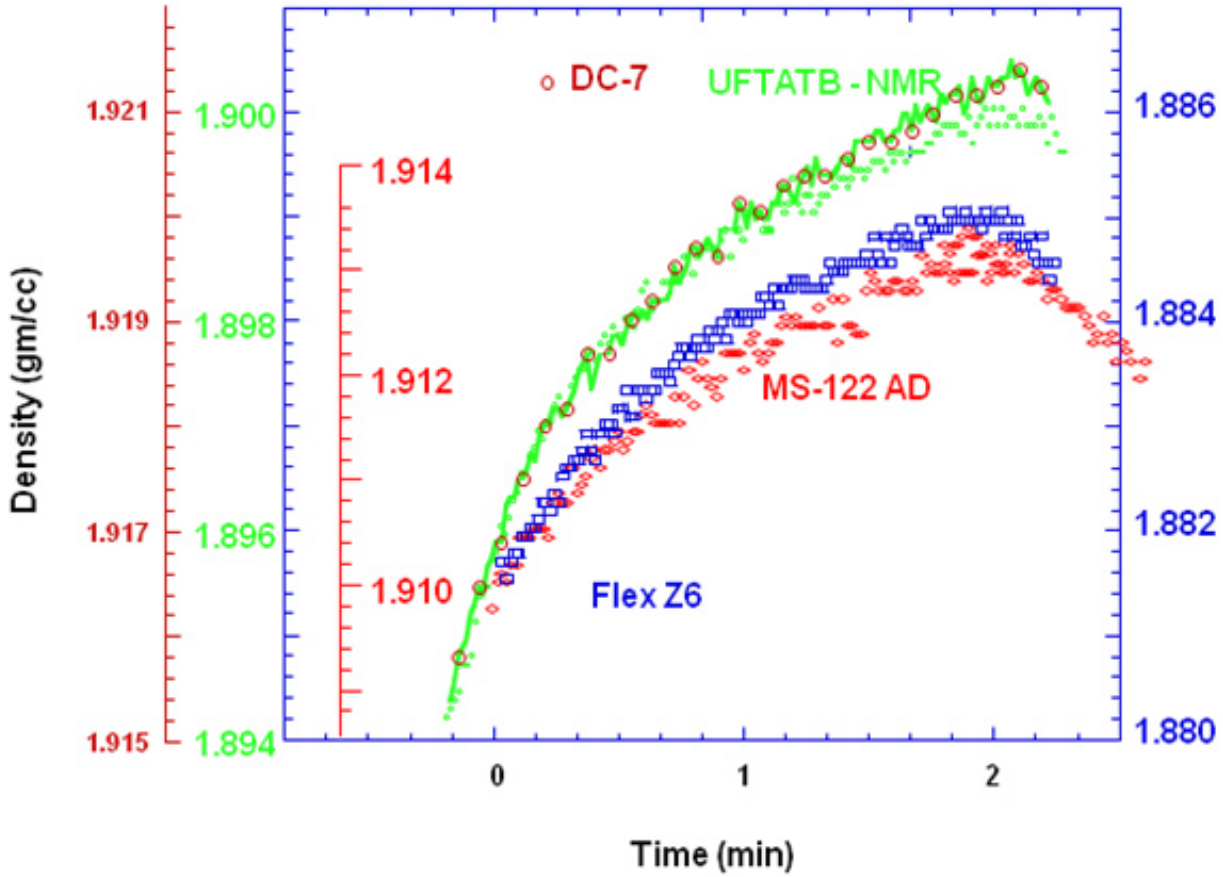

Figure 6. The density of UF TATB increased during the 2 minute dwell time at constant pressure (30 ksi) more than the increase associated with mold release in the die! The mold released samples tend to densify less during the hold, but the relative shape of the curve is very similar.

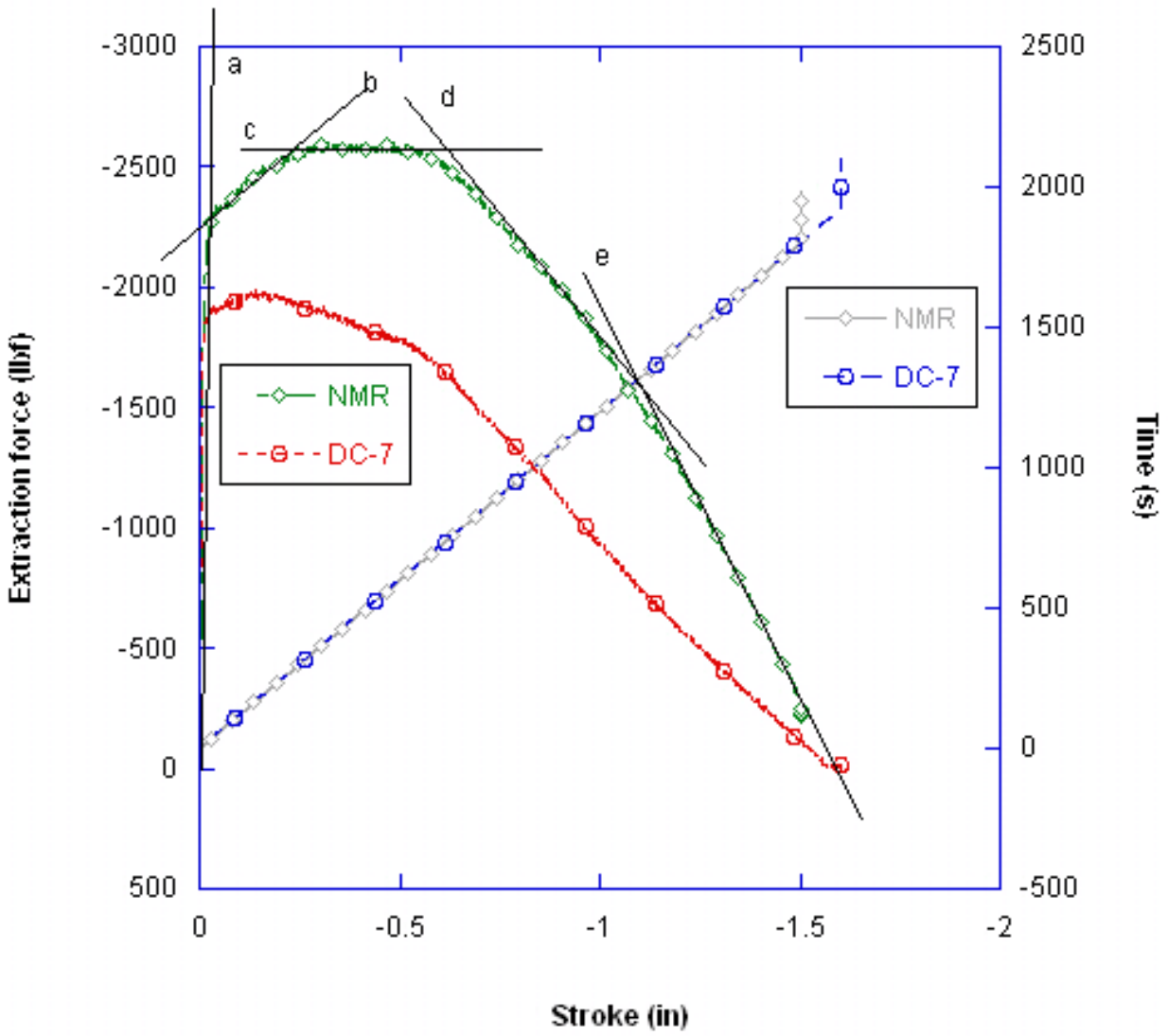

Figure 7. The maximum force required to extract a1/2" dia. x 1" penterythritol pellet was reduced by 700 lbf when the silicone mold release DC-7 was used.

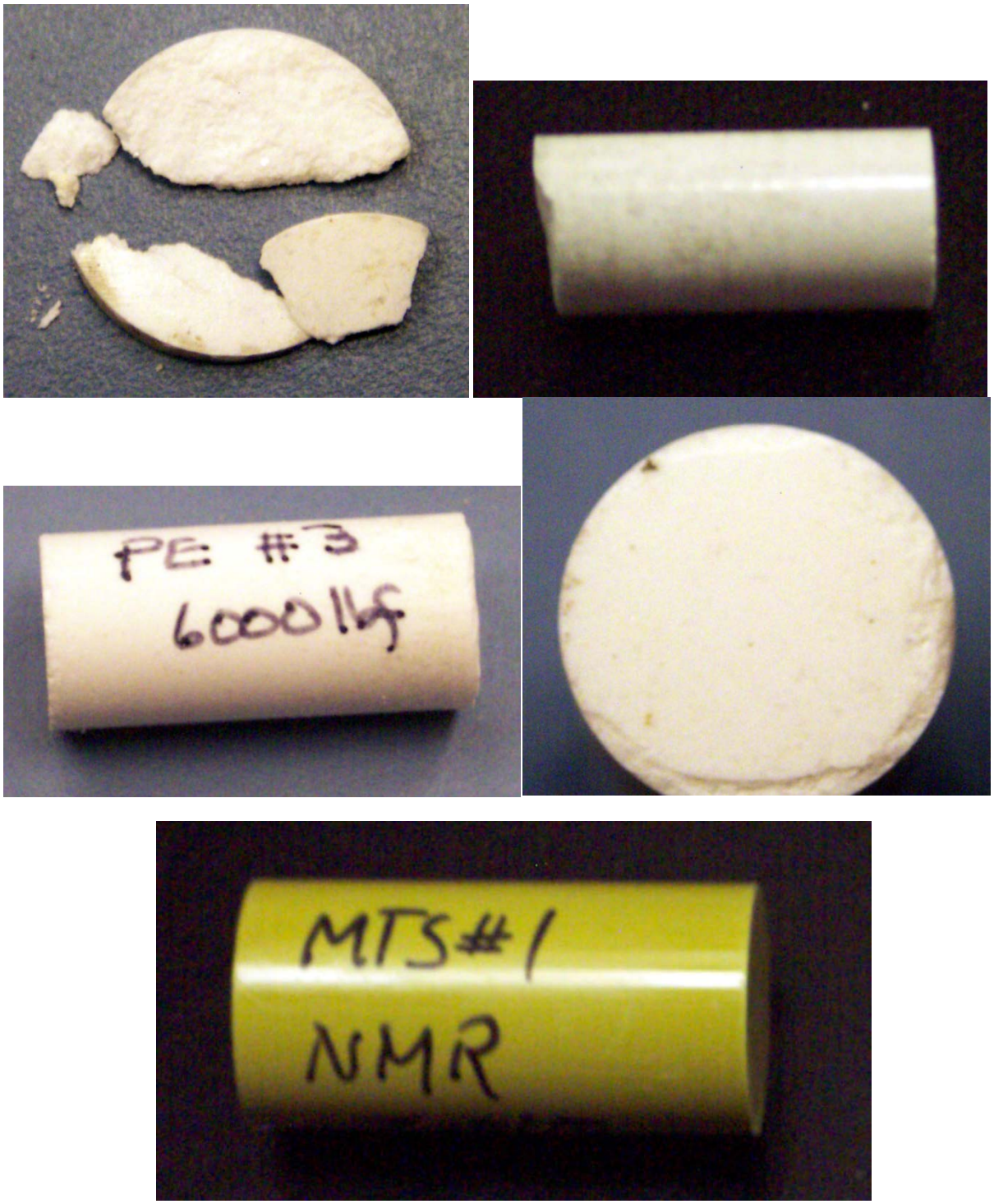

Figure 8. The bottoms of PEY molded parts without DC-7 mold release agent had laminar cracks (upper photos). When release agent was used, cracks were substantially reduced (middle photos). UF TATB (bottom photo) had no observable cracks.

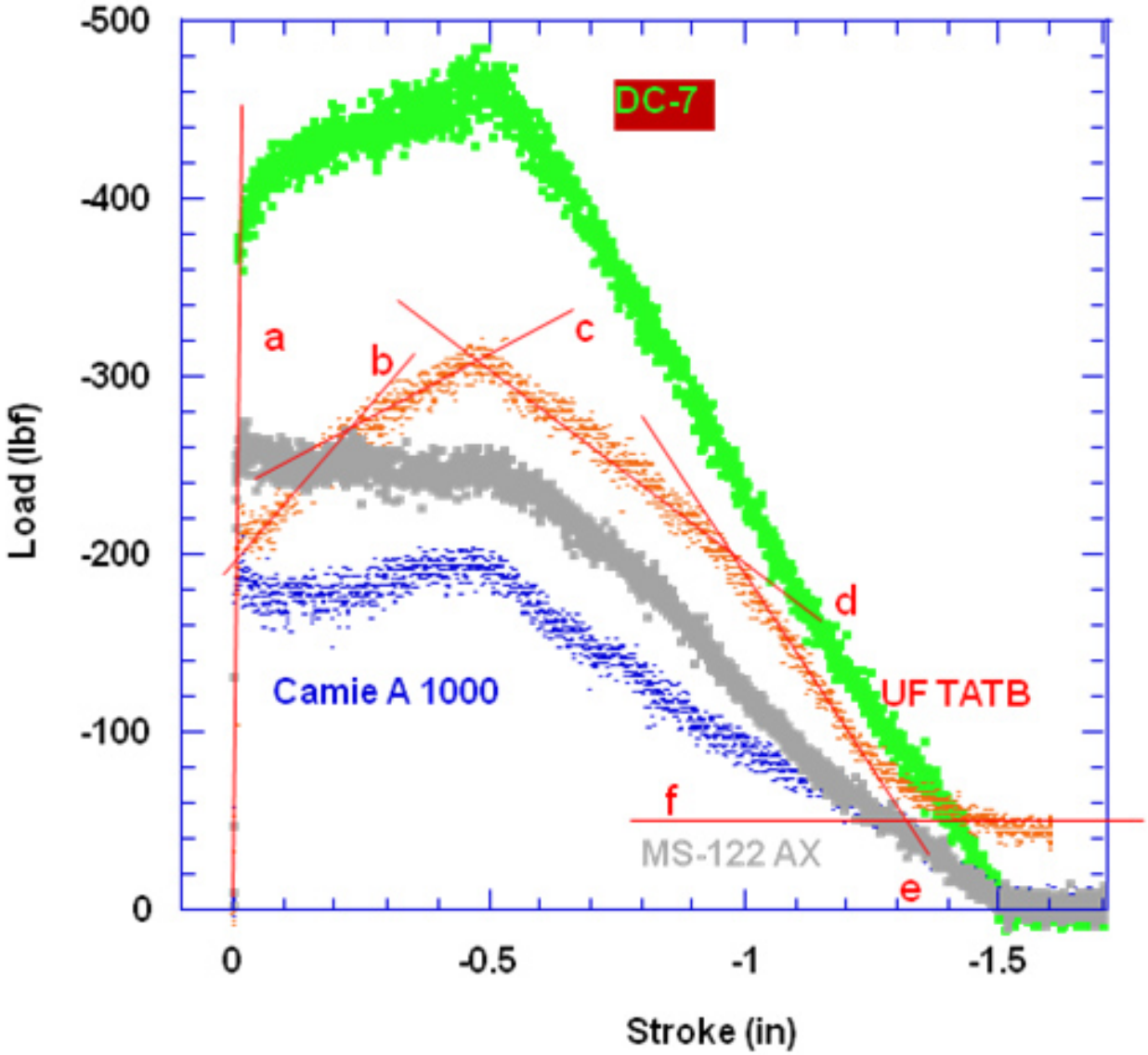

Figure 9. Comparison of extraction characteristics of 3 mold releases to UF TATB showed a rapid initial rise in extraction force followed by a constant or increasing force as the part moved out of the die. As the part begins to exit the die, all extractions except MS-122AX showed a peak followed by a linear or 2 step decrease in extraction force until the part exits the die at zero.

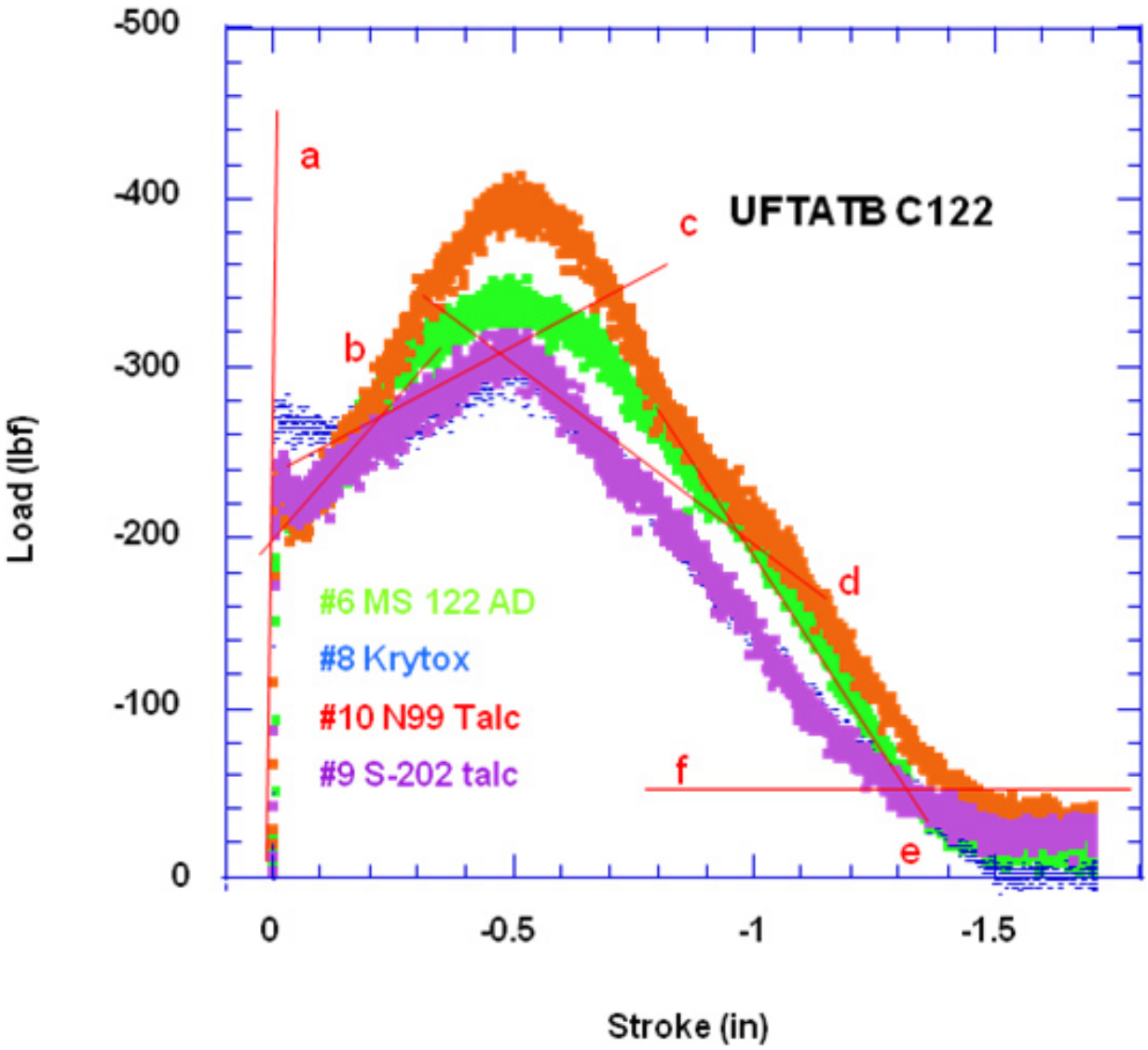

Figure 10. Extraction curves of 4 different mold releases were similar to neat UF TATB (lines a, b, c, d, e, and f (in red).

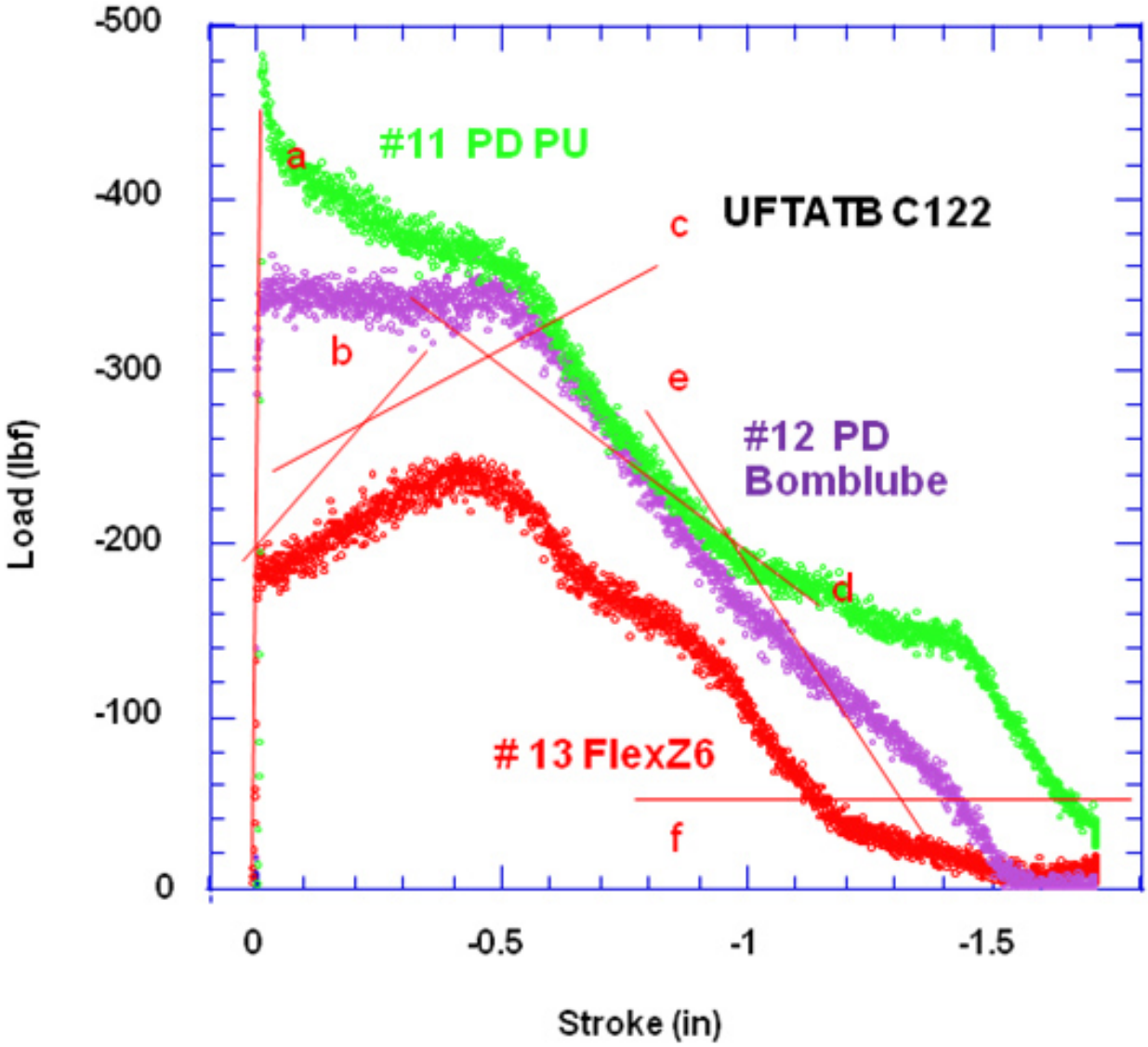

Figure 11. Extraction curves for urethane #11, silicone #12, and wax #13 based release agents were significantly different than neat UF TATB (lines a, b, c, d, e, and f).

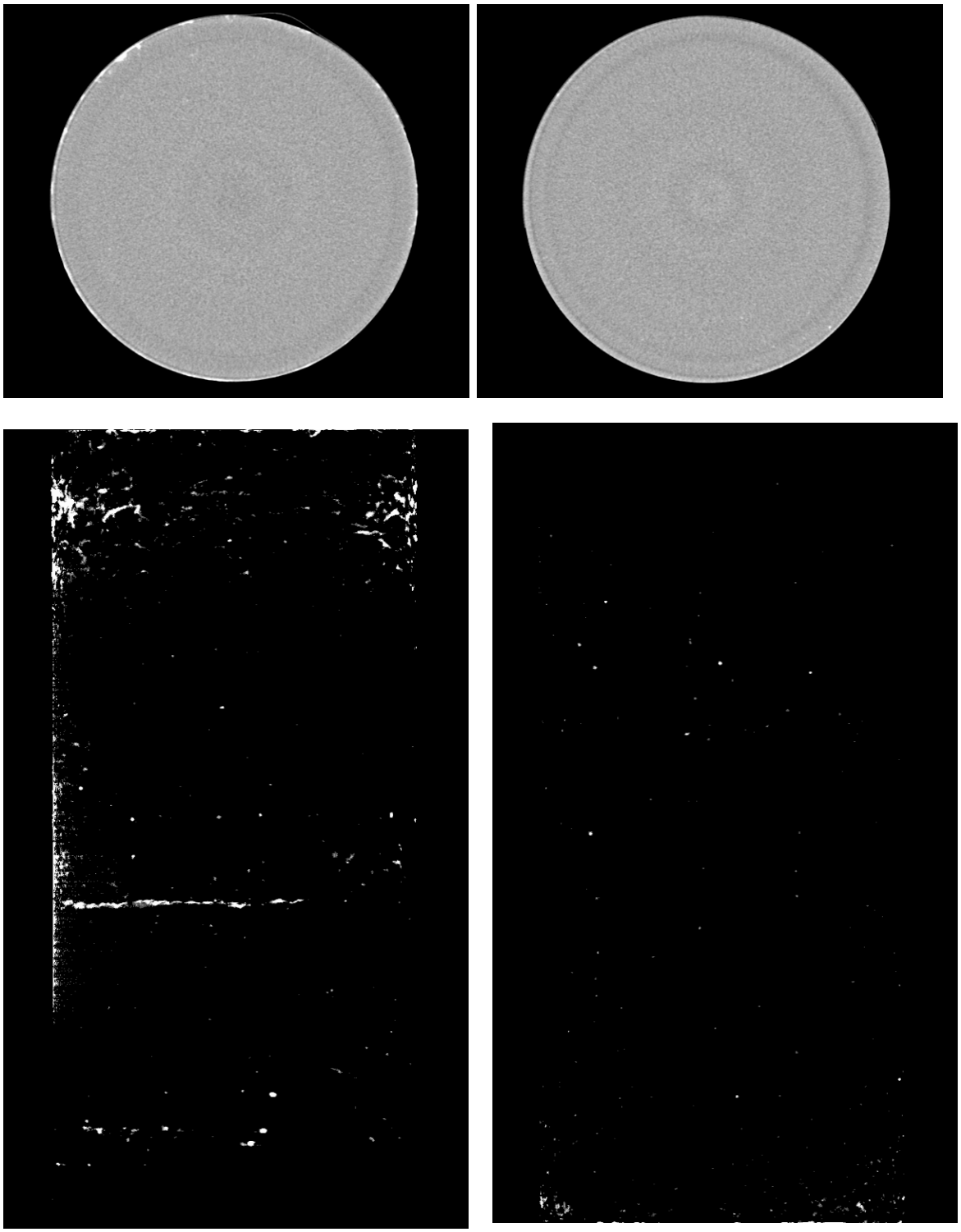

Figure 12. X-ray CT scan of UF TATB pressed part with spherical talc (#9 – LHS) and platy talc (#10 – RHS) imbedded near the surface. The non-uniform distribution of talc (white areas in the X-ray slice) suggests it is not evenly coated over the mold surface or has moved during compaction. Why the spherical talc incorporates more than platy talc is unknown.

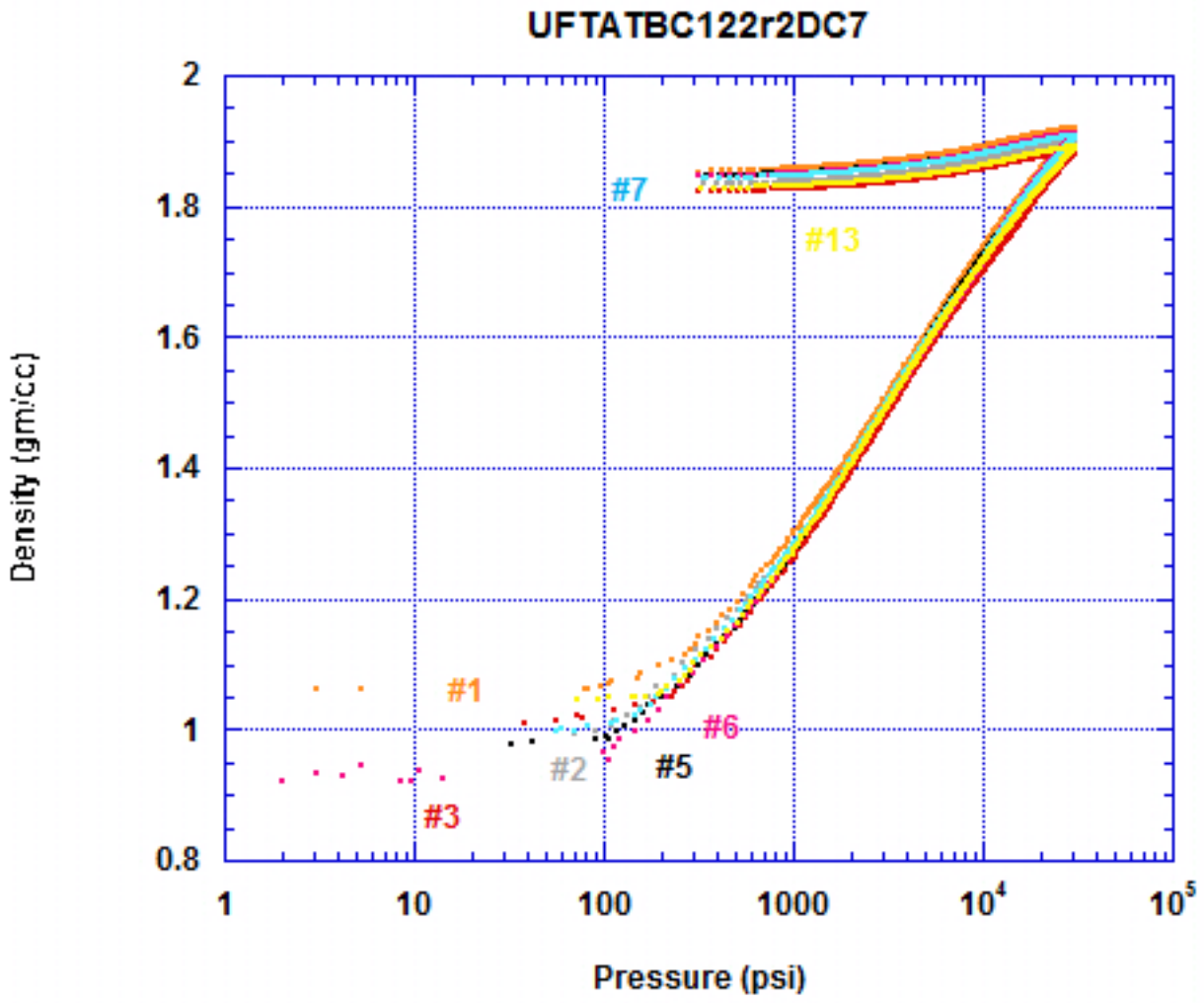

Figure 13. Walker-Bal'shin plots for the compaction of UF TATB without mold release (#1) and with 6 different mold release agents were very similar. Early densification, up to ~300 psi occurs by void filling, mid range compaction (300 < P < 7000 psi) is believed to be consolidation of aggregates and high pressure compaction, 7000 < P < 30,000 psi) is due to yielding and flow of TATB crystals.

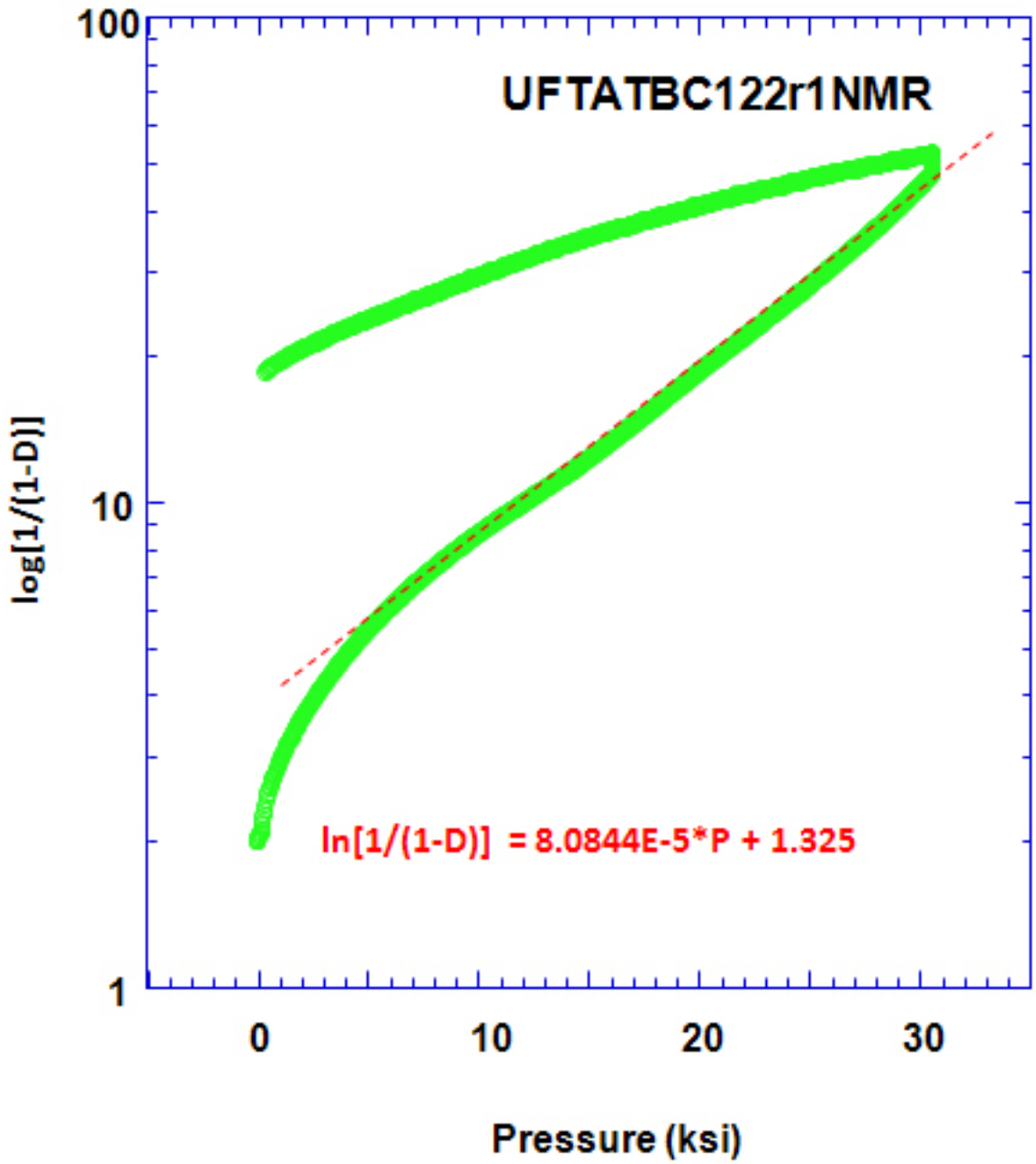

Figure 14. The linear portion of the Heckel Equation applied to the compaction phase provides an estimate of the yield pressure of the uf TATB particles as 1/slope = 7.83 MPa (1100 psi). Similar arguments for 3 stages of compaction are seen: low pressure (0 < P < 300 psi); mid range (300 < P <15000 psi) and high pressure (15 < P < 30 ksi)

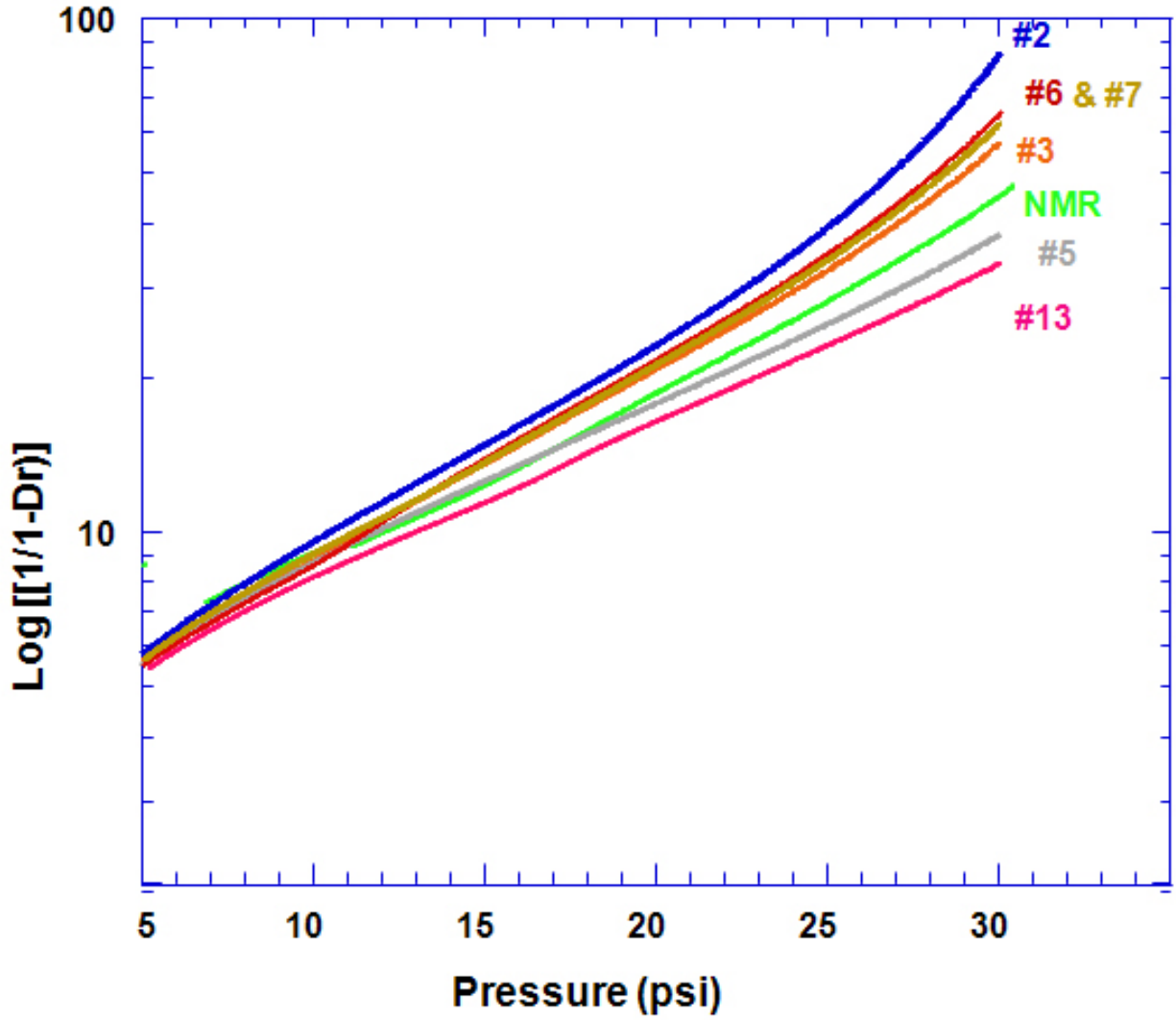

Figure 15. The "linear" section of the Heckel plots (taken as 5000 < P < 30,000 psi) for 6 mold released data sets behave slightly differently than unreleased TATB. The mold release agents are identified by the numbers in Table 1. The "linear" portion was fitted by the least squares method and the data compiled in Table 4. Estimates of the yield pressure were between 70 < Py < 105 MPa (9-15 ksi) and the relative density for particle deformation to begin was between 67 > D_a >77%.

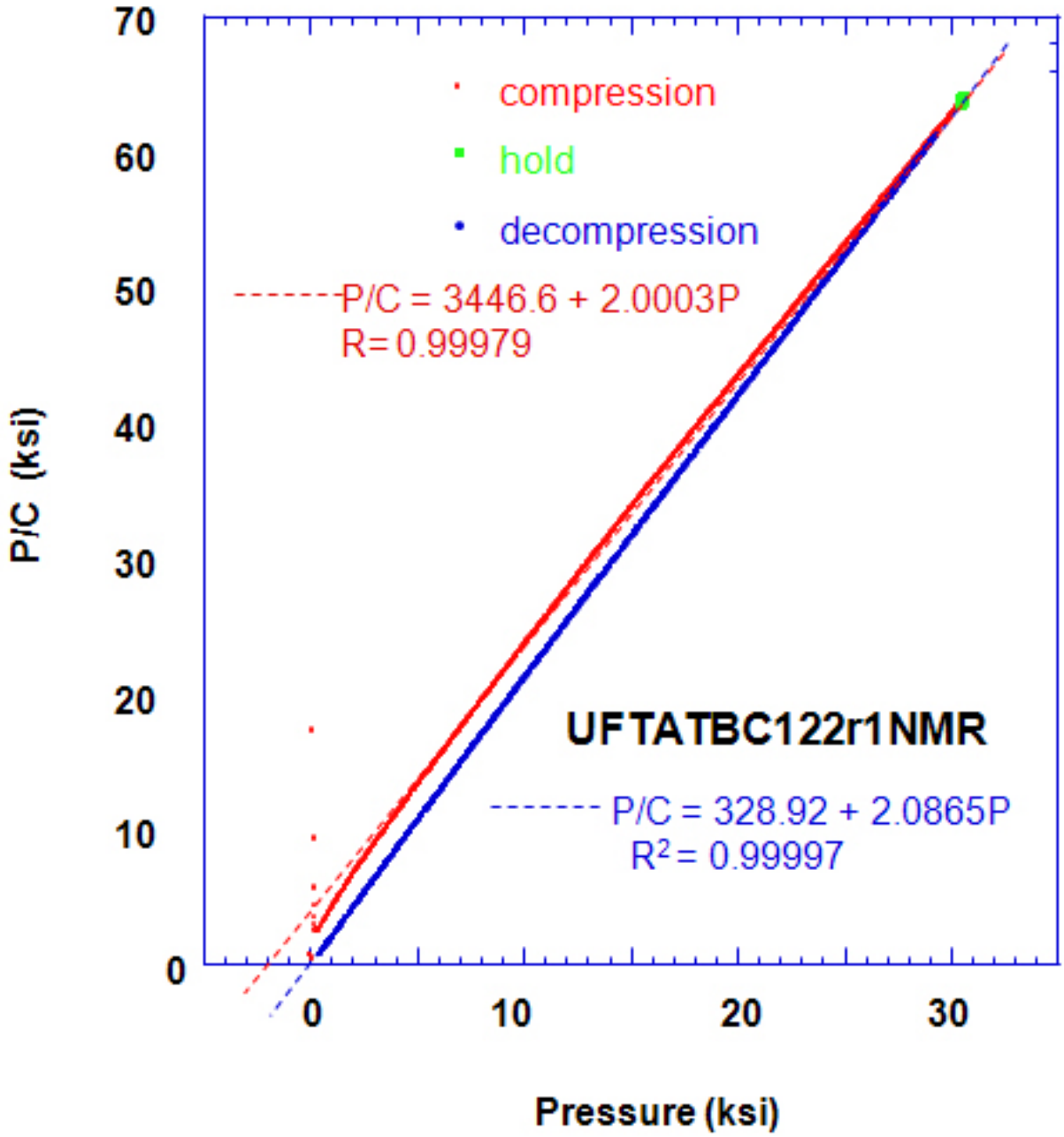

Figure 16. The Kawakita-Ludde equation fits both the compaction trace (red) and the pressure release curve (blue) for the unreleased UF TATB data. The green points at the top are from the pressure hold at 30 ksi. Note several data points during the early part of the compression cycle were anamolous and were ignored for fitting purposes. Also, the initial portion of the compression trace (red) deviates from linearity.

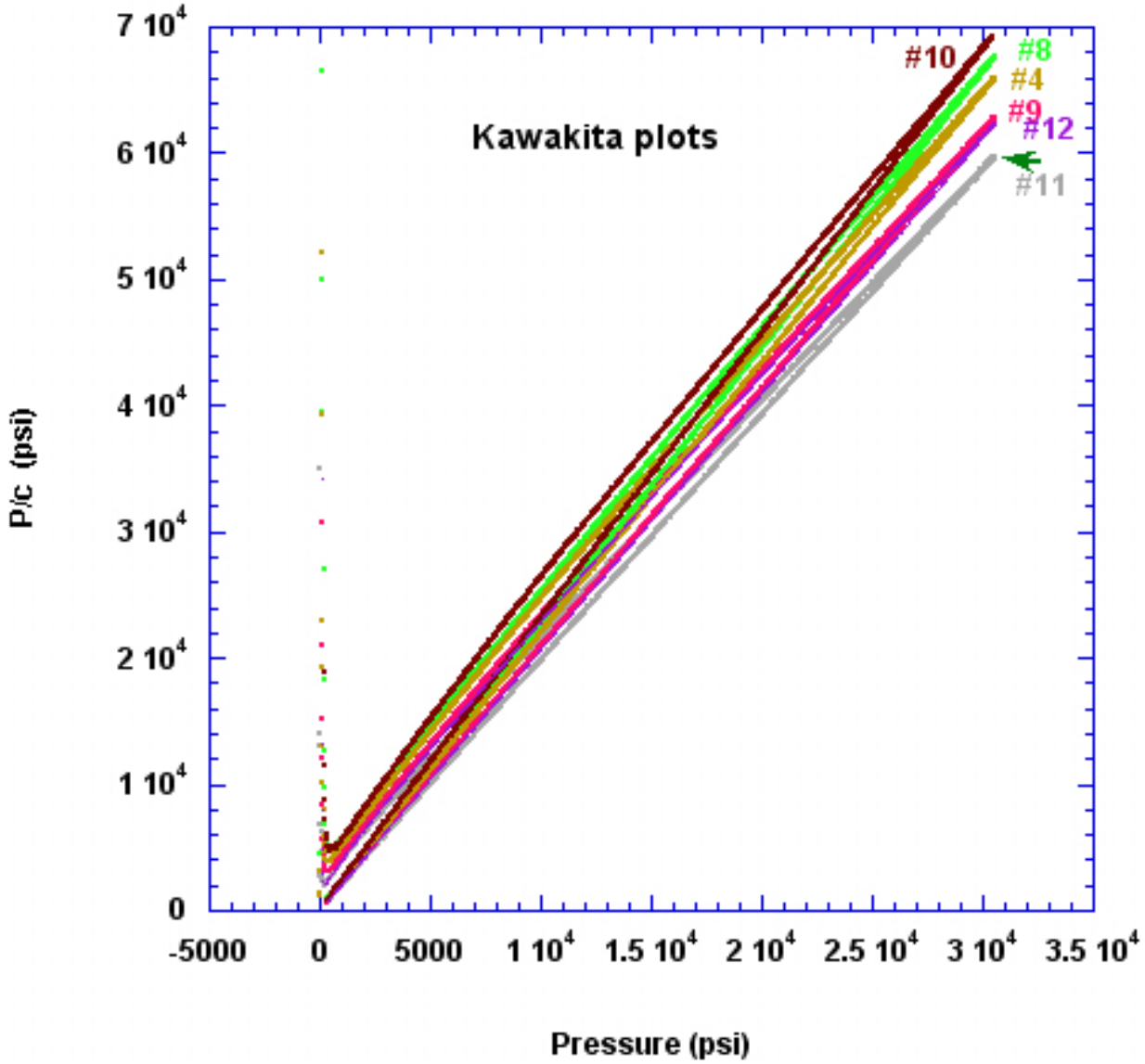

Figure 17. The Kawakita-Ludde equation was used for the various compression and decompression traces in this study. Shown above are 6 examples. Platy talc (#10), which is currently used, had different compaction and release characteristics than spherical talc (9).